PAPER • OPEN ACCESS

Validation of D–T fusion power prediction capability against 2021 JET D–T experiments

OPEN ACCESS
IOP Publishing | International Atomic Energy Agency
Nuclear Fusion
Nucl. Fusion **63** (2023) 112004 (21pp)
https://doi.org/10.1088/1741-4326/ace26d

Validation of D–T fusion power prediction capability against 2021 JET D–T experiments

Hyun-Tae Kim[1,*], Fulvio Auriemma[2], Jorge Ferreira[3], Stefano Gabriellini[4], Aaron Ho[5], Philippe Huynh[6], Krassimir Kirov[1], Rita Lorenzini[2], Michele Marin[7], Michal Poradzinski[1], Nan Shi[8], Gary Staebler[8], Žiga Štancar[1], Gediminas Stankunas[9], Vito Konrad Zotta[4], Emily Belli[8], Francis J Casson[1], Clive D Challis[1], Jonathan Citrin[5], Dirk van Eester[10], Emil Fransson[11], Daniel Gallart[12], Jeronimo Garcia[6], Luca Garzotti[1], Renato Gatto[4], Joerg Hobirk[13], Athina Kappatou[13], Ernesto Lerche[10], Andrei Ludvig-Osipov[11], Costanza Maggi[1], Mikhail Maslov[1], Massimo Nocente[14], Ridhima Sharma[1], Alessandro Di Siena[13], Par Strand[11], Emmi Tholerus[1], Dimitriy Yadykin[11] and JET Contributors[a]

[1] UKAEA, Abingdon, United Kingdom of Great Britain and Northern Ireland
[2] Consorzio RFX, corso Stati Uniti, 4, Padova 35127, Italy
[3] Instituto de Plasmas e Fusão Nuclear, Instituto Superior Técnico, Universidade de Lisboa, 1049-001 Lisboa, Portugal
[4] Sapienza University of Rome, Rome, Italy
[5] Dutch Institute for Fundamental Energy Research (DIFFER), PO Box 6336, 5600 HH Eindhoven, Netherlands
[6] IRFM, CEA F-13108, Sant-Paul-lez-Durance, France
[7] SPC, Swiss Plasma Center, Ecole Polytechnique Federale de Lausanne, Station 13, Lausanne 1015, Switzerland
[8] General Atomics, PO Box 85608, San Diego, CA 92186-5608, United States of America
[9] Lithuanian Energy Institute, Laboratory of Nuclear Installation Safety, Breslaujos Str. 3, LT-44403 Kaunas, Lithuania
[10] LPP-ERM/KMS, Association EUROFUSION-Belgian State, TEC partner, Brussels, Belgium
[11] Department of Space, Earth and Environment, Chalmers University of Technology, Gothenburg, Sweden
[12] Barcelona Supercomputer Center, Barcelona, Spain
[13] Max-Planck Institut für Plasmaphysik Garching, Germany
[14] Department of Physics 'G. Occhialini', University of Milano-Bicocca, 20126 Milan, Italy

E-mail: Hyun-Tae.Kim@ukaea.uk

Received 15 March 2023, revised 24 May 2023
Accepted for publication 28 June 2023
Published 12 October 2023

Abstract

JET experiments using the fuel mixture envisaged for fusion power plants, deuterium and tritium (D–T), provide a unique opportunity to validate existing D–T fusion power prediction capabilities in support of future device design and operation preparation. The 2021 JET D–T

[a] See the author list of "Overview of T and D-T results in JET with ITER-like wall" by C.F. Maggi *et al* to be published in *Nuclear Fusion Special Issue: Overview and Summary Papers from the 29th Fusion Energy Conference (London, UK, 16–21 October 2023).*

[*] Author to whom any correspondence should be addressed.

experimental campaign has achieved D–T fusion powers sustained over 5 s in ITER-relevant conditions i.e. operation with the baseline or hybrid scenario in the full metallic wall. In preparation of the 2021 JET D–T experimental campaign, extensive D–T predictive modelling was carried out with several assumptions based on D discharges. To improve the validity of ITER D–T predictive modelling in the future, it is important to use the input data measured from 2021 JET D–T discharges in the present core predictive modelling, and to specify the accuracy of the D–T fusion power prediction in comparison with the experiments. This paper reports on the validation of the core integrated modelling with TRANSP, JINTRAC, and ETS coupled with a quasilinear turbulent transport model (Trapped Gyro Landau Fluid or QualLiKiz) against the measured data in 2021 JET D–T discharges. Detailed simulation settings and the heating and transport models used are described. The D–T fusion power calculated with the interpretive TRANSP runs for 38 D–T discharges (12 baseline and 26 hybrid discharges) reproduced the measured values within 20%. This indicates the additional uncertainties, that could result from the measurement error bars in kinetic profiles, impurity contents and neutron rates, and also from the beam-thermal fusion reaction modelling, are less than 20% in total. The good statistical agreement confirms that we have the capability to accurately calculate the D–T fusion power if correct kinetic profiles are predicted, and indicates that any larger deviation of the D–T fusion power prediction from the measured fusion power could be attributed to the deviation of the predicted kinetic profiles from the measured kinetic profiles in these plasma scenarios. Without any posterior adjustment of the simulation settings, the ratio of predicted D–T fusion power to the measured fusion power was found as 65%–96% for the D–T baseline and 81%–97% for D–T hybrid discharge. Possible reasons for the lower D–T prediction are discussed and future works to improve the fusion power prediction capability are suggested. The D–T predictive modelling results have also been compared to the predictive modelling of the counterpart D discharges, where the key engineering parameters are similar. Features in the predicted kinetic profiles of D–T discharges such as underprediction of n_e are also found in the prediction results of the counterpart D discharges, and it leads to similar levels of the normalized neutron rate prediction between the modelling results of D–T and the counterpart D discharges. This implies that the credibility of D–T fusion power prediction could be *a priori* estimated by the prediction quality of the preparatory D discharges, which will be attempted before actual D–T experiments.

Keywords: JET D–T, fusion power prediction, TGLF, QuaLiKiz, TRANSP, JINTRAC, ETS

(Some figures may appear in colour only in the online journal)

1. Introduction

Reliable deuterium and tritium (D–T) fusion power prediction is important to optimize D–T operation scenarios and to design future D–T fusion reactors. Predicting fusion power is a challenging task as it is very sensitive to plasma parameters. Thermal D–T fusion reaction rate scales faster than a linear increase with fuel ion density and temperature. It thus requires sophisticated integrated modelling that correctly predicts the plasma parameters by modelling the heating and transport in a plasma. To ensure trustworthy prediction, it is essential to quantitatively assess the present prediction modelling tools using existing experimental data and to identify improvements required in the prediction models.

Such a validation, nevertheless, has not been possible until now due to the lack of D–T experimental data in present devices. The previous D–T experimental campaign was in 1997 at JET [1, 2]. The objectives in most D–T discharges at that time were, however, to produce transient high performance pulses, which were operated with edge-localized-mode (ELM)-free H-mode regime or optimized shear regime [1]. Such transient discharges are not directly relevant to ITER D–T discharges, where stationary operation is one of the key objectives. Although there were a small number of stationary H-mode discharges in 1997 [3], the quality of experimental data is not good enough to quantitatively validate the predictive modelling.

In addition, ITER is designed to have a fully metallic wall (i.e. beryllium first wall and tungsten divertor), whereas all the D–T discharges in 1997 were operated with the carbon plasma facing components. In 2011 the previous carbon wall in JET was replaced with an ITER-like full metallic wall to produce a similar environment surrounding the plasma as ITER [4]. It has been reported in JET and ASDEX-U that the plasma energy confinement is affected by the presence of a metal wall [5, 6]. Therefore, since the refurbishment of the wall, plasma operations with JET's ITER-like wall have been extensively explored [7–9] and demonstrated the two main operating scenarios envisaged for ITER (baseline and hybrid scenarios, defined in section 3.1).

With the optimized operating scenarios, EURO*fusion* carried out the second JET D–T experimental campaign in 2021, and achieved D–T fusion power sustained over 5 s under the ITER-relevant conditions [10]. As no further D–T experimental campaigns are foreseen in any other ITER partner's current facilities before the ITER D–T experiments[15], the JET D–T experimental campaign in 2021 provides a unique opportunity to validate the current D–T fusion power prediction capability before the ITER D–T experiments take place. To improve the validity of ITER D–T predictive modelling, it is important to specify the accuracy of D–T fusion power predictions with respect to the measured values in 2021 JET D–T discharges, to document the models and simulation settings used in the predictive integrated modelling, and to suggest further improvements needed in the present prediction tools. It has motivated modelling activities organized in the JET D–T scenario extrapolation task.

This paper reports on the *collective* modelling of the achieved high performance JET D–T plasmas. There are several integrated modelling codes actively used in the fusion community (e.g. TRANSP [11, 12], JINTRAC [13], and ETS [14]) that can predict the kinetic profiles and the fast particle population. Each code uses different heating and transport models, which will be introduced in section 3.2. In addition, even the numerical algorithm to solve the energy and particle balance equations in the integrated modelling codes are also not identical [15]. For example, TRANSP solves the equation for electron particle balance (and ion particle densities are calculated with the quasi-neutrality assumption), while JINTRAC and ETS solves the equation for each ion particle balance (and electron particle density is calculated with the quasi-neutrality assumption) [15]. These differences could cause different fusion power predictions. To address the uncertainty resulting from the choice of modelling codes, D–T fusion power has been computed with the three integrated modelling codes, which are coupled to the two mainstream quasilinear turbulent transport models, Trapped Gyro Landau Fluid (TGLF) or QuaLiKiz (i.e. TRANSP-TGLF, JINTRAC-TGLF, JINTRAC-QuaLiKiz, and ETS-TGLF). Using identical input data and standard simulation settings, the integrated modelling codes simulated the best performing D–T baseline and hybrid discharges from the 2021 JET D–T campaign. The predicted D–T fusion powers were compared between codes and with the measured fusion power.

In order to improve the chances of success in the D–T experimental campaign, it was necessary to optimise the planned operating scenarios with D discharges during the previous years [16], using predictive modelling to guide the experiments [17–22]. Similarly, ITER D–T operational scenarios need to be developed with D discharges beforehand, with intensive D–T discharge predictive modelling based on the achieved D discharges. An important question is whether the quality of predictive modelling of preparatory D discharges (i.e. how well they predict the kinetic profiles and the neuron rates) can be used as a good indicator of the quality of the D–T discharge prediction, and in particular whether features of D predictive modelling are also apparent in the D–T predictive modelling. This motivated attempts to correlate the prediction quality of D discharges with that for the 2021 campaign D–T discharges. D discharges with the engineering parameters, which are similar to the high fusion power baseline and hybrid D–T discharges, were selected, and their predictive integrated modelling results were compared to the D–T discharge modelling results.

This paper is structured as follows in order to outline the validation of current D–T fusion power prediction capability. In section 2, to assess uncertainties of fusion power prediction separately from the kinetic profile prediction, D–T fusion power calculated with interpretive TRANSP runs are statistically compared to the measured values. In section 3.1, two high performance D–T discharges and their counterpart D discharges that were used for predictive integrated modelling are introduced. In section 3.2, the predictive integrated modelling codes are introduced together with description of the heating and transport models. In section 3.3, the D–T fusion power prediction results are presented, together with the modelling results of kinetic profiles and the heat and particle source profiles. In section 3.4, candidates for the JET D–T fusion power underprediction and foreseen uncertainties in the prediction of fusion power in ITER are discussed, and future work is suggested. Section 4 provides the conclusion.

2. D–T fusion power calculation with interpretive integrated modelling

D–T fusion power is a function of multiple plasma parameters. In principle, it can be calculated with the following formula:

$$\begin{aligned} P_{\mathrm{fus}}[\mathrm{MW}] = \Bigg(& \int n_{\mathrm{th},D} n_{\mathrm{th},T} < \sigma v > (T_{\mathrm{D}}, T_{\mathrm{T}}) \mathrm{d}V \\ & + \int n_{\mathrm{th},D} n_{\mathrm{fast},T} < \sigma v > (T_{\mathrm{D}}, E_{\mathrm{fast},T}) \mathrm{d}V \\ & + \int n_{\mathrm{th},T} n_{\mathrm{fast},D} < \sigma v > (T_{\mathrm{T}}, E_{\mathrm{fast},D}) \mathrm{d}V \\ & + \int n_{\mathrm{fast},D} n_{\mathrm{fast},T} < \sigma v > (E_{\mathrm{fast},D}, E_{\mathrm{fast},T}) \mathrm{d}V \Bigg) \\ & \times 17.6 \times 1.6 \times 10^{-19} \end{aligned} \quad (1)$$

where n_{th} and n_{fast} are the thermal and the NBI fast ion density, T_{D} and T_{T} are the temperature of D and T thermal ions, and E_{fast} is the fast ion energy. $17.6 \times 1.6 \times 10^{-19}$ is the fusion energy per D–T fusion reaction in the unit of [MJ]. In equation (1) the first term is the thermonuclear fusion power, the second and the third terms are the beam-thermal fusion power, and the last term is the beam–beam fusion power. The first term is only a function of ion temperature and density, while the other terms require NBI heating models (and ICRF heating models to simulate fast ion acceleration by RF wave),

[15] Planned in the 2030 s.

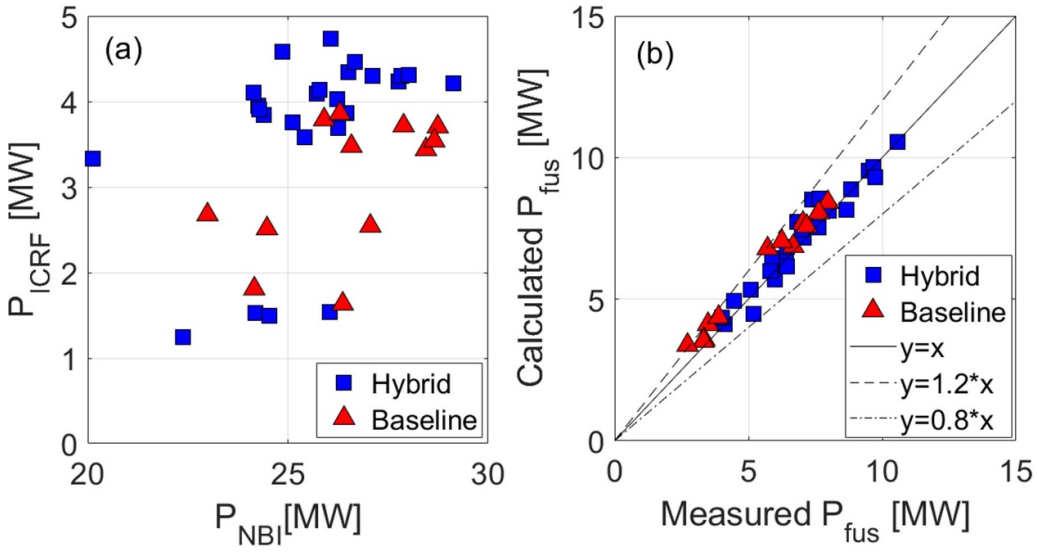

Figure 1. (*a*) NBI and ICRF heating power in the database (*b*) D–T fusion power calculation with interpretive TRANSP for JET DTE2 discharges [25, 26].

which simulate the slowing-down process of fast ions. The fourth term is typically much smaller than the other terms, and in most JET discharges it is small enough to ignore.

As can be seen in equation (1), fusion power calculation requires integrated modelling, which involves the fusion cross sections and several physics models e.g. NBI heating, ICRF heating, turbulent transport, fast ion population, and equilibrium, which are functions of kinetic profiles. Interpretive TRANSP runs calculate the fusion power with prescribed kinetic profiles (i.e. measured ion temperature and inferred ion density from measured n_e) and the internal NBI heating model i.e. NUBEAM [23, 24]. Use of measured kinetic profiles is the main difference compared to the predictive modelling, where the fusion power is calculated with the predicted kinetic profiles. Even with measured kinetic profiles, fusion power calculation in the interpretive simulations could have additional uncertainties due to the measurement error bars in kinetic profiles and prescribed impurity content, and the calculation error bars in the beam-thermal fusion reaction modelling and the equilibrium modelling for the volume integration of fusion reactions. To estimate these uncertainties, interpretive TRANSP runs have been performed for 12 baseline ($I_p = 3.0 - 3.5$[MA], $B_T = 2.8 - 3.3$[T], $P_{\mathrm{NBI}} = 23 - 28.7$[MW], and $P_{\mathrm{ICRF}} = 1.6 - 3.9$[MW]) and 26 hybrid discharges ($I_p = 2.3$[MA], $B_T = 3.4$[T], $P_{\mathrm{NBI}} = 19.7 - 29.1$[MW], and $P_{\mathrm{ICRF}} = 1.2 - 4.7$[MW]), which were selected based on the good diagnostics data. The ratio of fuel gas mixture in the discharges was measured to be about 50%D and 50%T mixture with edge H,D,T-alpha spectroscopy. The initial ratio of the fuel ion mixture in the interpretive TRANSP runs was assumed with the measured data, and the slight evolution of D and T ion ratio due to the NBI beam fuelling was consistently calculated in the interpretive TRANSP. Figure 1(*a*) shows the range of the NBI and ICRF heating power in the discharges, and table 4 in appendix A lists the shot numbers, operation scenarios, and time windows in each discharge. The interpretive TRANSP runs were made with a standard simulation setting and a common procedure for experimental input data preparation. The details of the interpretive TRANSP runs and modelling results with a wider range of discharges (e.g. different RF scheme, T-rich discharges) can be found in [25, 26]. Figure 1(*b*) shows that all of the fusion power calculated in the 38 D–T discharges are located within 20% error bars to the measured values. This indicates that with prescribed kinetic profiles the fusion power can be modelled to within an accuracy of 20%.

Figures 2(*a*) and (*b*) shows the thermonuclear fusion power and the beam-thermal fusion power, calculated in the interpretive TRANSP simulations. At the same total fusion power, the baseline discharges have higher thermonuclear fusion power than the hybrid discharges, and vice versa for the beam-thermal fusion power. This is due to the higher ion density in the baseline discharges, which is a typical feature of the high I_p operation. In both high performance D–T baseline and hybrid discharges, the increase in the total fusion power was mainly driven by the increase in the NBI heating power, with the beam-thermal fusion power and thermonuclear fusion power both increasing with NBI heating. Since the latter increases more rapidly, in both scenarios the ratio of the thermonuclear fusion power to the total fusion power increases with the total fusion power (see figure 2(*c*)). The highest thermonuclear contribution to the total fusion yield of more than 50% was observed in the highest performing baseline discharges. This suggests that the thermonuclear contribution should be dominant in the higher performance baseline or hybrid operation regime, planned in ITER.

NUBEAM in TRANSP, which will be introduced more in detail in section 3.2, simulates the slowing down of the alpha particles with the Monte-Carlo method using the same approach as for the NBI ions. Figure 2(*d*) shows the alpha

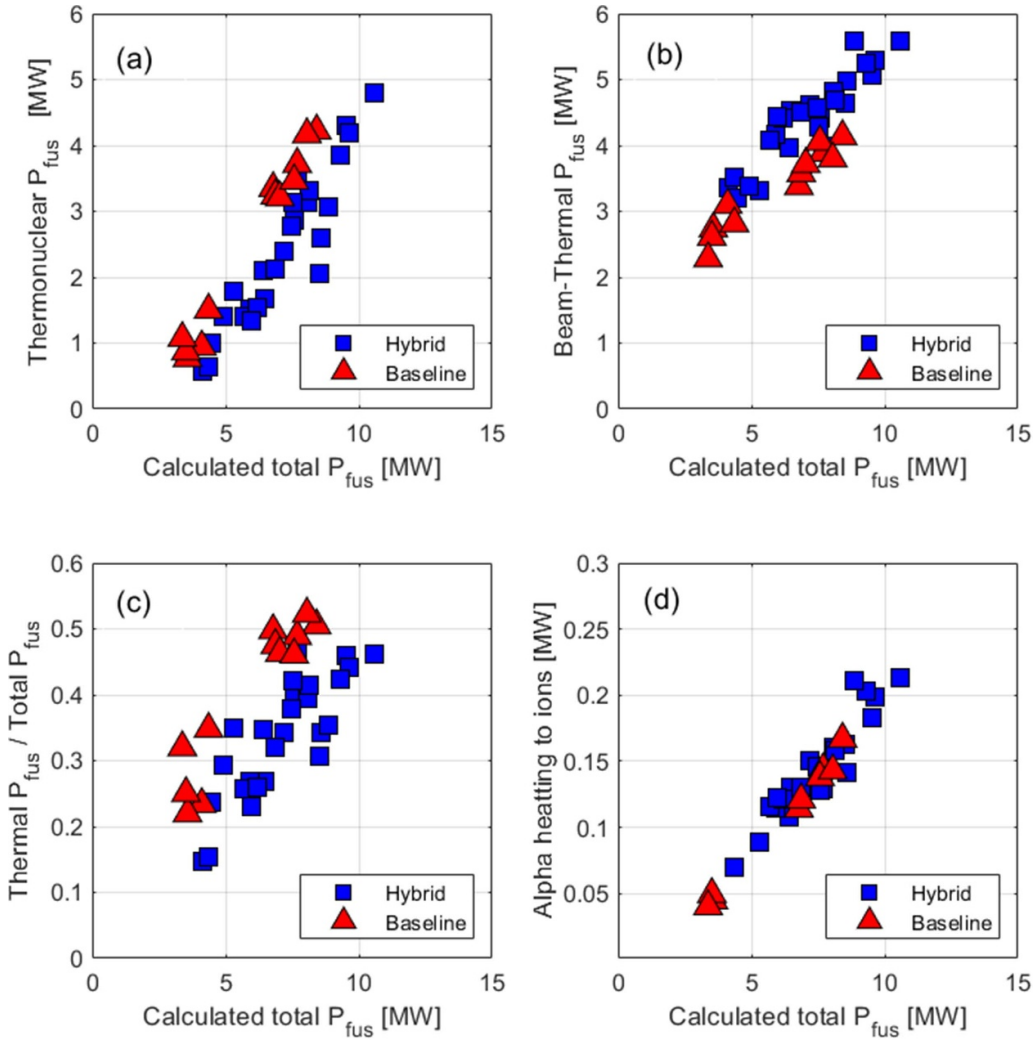

Figure 2. (*a*) The thermonuclear fusion power (*b*) the beam-thermal fusion power, (*c*) the ratio of the thermal neutron rate to the total neutron rate, and (*d*) alpha heating power to ions, calculated in the interpretive TRANSP.

heating to ions calculated in the interpretive TRANSP simulations. The calculated alpha heating power to ions linearly increases with the total fusion power. However, the amount of the alpha heating is very small (i.e. $<$0.25 MW) and thus is unlikely to have any significant effects on T_i profiles, though the alpha heating is modelled in the predictive integrated modelling in this paper.

3. D–T fusion power calculation with predictive integrated modelling

3.1. Reference discharges

ITER has two main operating scenarios i.e. baseline and hybrid scenario. These scenarios were used as the main operating scenarios in 2021 JET D–T experimental campaign. The baseline scenario pursues high plasma performance at high I_p and B_T, and relaxed J_p profiles ($\beta_N - 1.8$, $q_{95} - 3$) [7, 27]. On the other hand, the hybrid scenario takes the advantages of the favourable confinement behaviour when operating at high β_N and the possibility to avoid performance degrading MHD with a tailored J_p profiles and $q_0 > 1$ ($\beta_N = 2 - 3$, $q_{95} - 4.8$) [28]. In preparation for JET D–T operation, the baseline and hybrid scenarios were extensively optimized with D discharges in the previous years [7, 9], and the optimized scenarios successfully demonstrated high performance D–T discharges with the ITER-Like wall in 2021 [27, 28]. Among the achieved D–T discharges, the reference baseline and hybrid D–T discharges which have 50%–50% D–T fuel mixture, a stationary time window, and high fusion performance were selected for predictive integrated modelling, aiming to assess our current fusion power prediction capability for ITER-relevant D–T discharges. The shot numbers and operation parameters are indicated in table 1.

The preparatory D discharges were also selected for comparison with the D–T discharges. The gold and blue lines in figure 3 are the time traces in the reference D–T discharges and the counterpart D discharges, respectively. As can be seen, the key engineering parameters such as I_p, B_T, the total heating power (i.e. $P_{\mathrm{NBI}} + P_{\mathrm{ICRF}} + P_\alpha$) are similar in the D–T

Table 1. Values of the time traces averaged over the analysis time window in the reference D–T discharges for predictive integrated modelling.

Operation scenario	Baseline D	Baseline D–T	Hybrid D	Hybrid D–T
Shot number	96 482	99 948	97 781	99 949
Time window(s)	50.0–50.5	49.5–50	49.0 – 49.5	48.75–49.25
D and T ratio	100 % and 0%	49% and 51%	100% and 0%	47% and 53%
I_p[MA]	3.5	3.5	2.3	2.3
B_T[T]	3.3	3.3	3.4	3.4
q_{95}	3.2	3.2	4.8	4.8
P_{NBI} [MW]	29.5	28.7	30	27
P_{ICRF}[MW]	4.9	3.6	2.9	4.2
P_α[MW]	0	1.5	0	1.25
ICRF scheme	H at N = 1 (dipole phasing)	H at N = 1 (dipole phasing)	H at N = 1 (dipole phasing)	H at N = 1 (dipole phasing)
H minority fraction $(= H/(H+D+T))$	4%	2%	3%	4%
Fuelling	D gas injection + D ELM pacing pellet	D–T gas injection + D ELM pacing pellet	D gas injection	D–T gas injection
$H98(y,2)$ [31]	0.74	0.83	0.95	0.93
Neutron rate $[\times 10^{18}\#/s]$	0.025	3	0.035	2.5

and D counterpart discharges[16]. The experimental data (e.g. pedestal values of T_i, T_e, and n_e) in the reference discharges were used as boundary conditions in the integrated transport modelling codes to calculate the kinetic profiles in the core ($0 \leqslant \rho \leqslant 0.85$), and the corresponding fusion power.

One of the main differences between the baseline and the hybrid discharge operation is the gas fuelling scheme. For ELM frequency control, the baseline D–T discharges require D ELM pacing pellets[17] in addition to D–T gas injection [29] whereas the hybrid discharges can maintain stable type-I ELM with D–T gas injection only. During the scenario optimization in previous years, it was found that low gas fuelling improves the ion heat confinement, allowing high fusion performance [8, 30]. However, low gas injection in the baseline discharges reduces the ELM frequency, increasing the risk of tungsten accumulation, thereby leading to disruption. Low gas operation in the baseline discharges was only possible when sufficient ELM frequency was maintained by using ELM pacing pellets.

The time windows for D–T fusion power prediction modelling have been selected to be 49.5–50 s[18] in 99 948 (Baseline, D–T) and 48.75–49.25 s in 99 949 (Hybrid, D–T), as they have the most stable maximum fusion performances in the discharges, which are 8.3 MW and 7.2 MW, respectively. As can be seen by the time traces of core T_e and n_e in figure 3, both time windows have approximately stationary plasma parameters. It should be, however, noted that 99 948 (Baseline, D–T) exhibits a gradual increase in core n_e. It resulted from the increase in the pedestal n_e due to the intermittency of ELM events, despite the use of ELM pacing pellets. The reduced ELM frequency led to reduced tungsten flushing and excessive radiation at the low field side, thereby terminating the discharge at 51.4 s.

The stationary time windows of the counterpart D discharges were selected to be 50.0–50.5 s in 96 482 (Baseline, D) and 49.0–49.5 s in 97 781 (Hybrid, D), respectively. Figure 4 compares the measured kinetic profiles between the D–T (gold) and D (blue) counterpart discharges. The major difference is the pedestal n_e. About 99 948 (Baseline, D–T) has a higher pedestal n_e than 96 482 (Baseline, D), leading to a higher n_e for a wide radial region in the core. The same feature is also seen in the hybrid discharges, but milder than the baseline discharges. In the hybrid discharges, T_i within $\rho \leqslant 0.2$ is higher in 97 781 (Hybrid, D) than in 99 949 (Hybrid, D–T). This could be due to the deeper penetration of D NBI beams than of T NBI beam, as D NBI beams have a higher speed than T NBI beams at the given NBI voltages. The NBI heat and particle deposition calculated with the interpretive TRANSP runs also consistently shows the higher core deposition in 97 781 (Hybrid, D) (see figure 9).

3.2. Predictive integrated modelling codes

3.2.1. Input data and simulation settings. Three integrated modelling codes TRANSP [11, 12], JINTRAC [13], and ETS [14], which have been used as the major tools in EURO*fusion* integrated modelling activities, were selected to evaluate the present D–T fusion power prediction capability and to assess the uncertainty that could result from the choice of modelling tools. Also, TGYRO developed in General Atomics has participated in the collective modelling to cross-benchmark

[16] Note, counterpart hybrid D–T discharges with more similar engineering parameters were achieved in August 2022, when the modelling work in this paper was already almost completed. The discharges were presented in [28].

[17] T pellets are not available to use for a technical reason.

[18] Plasma break-down takes place at 40 s in JET.

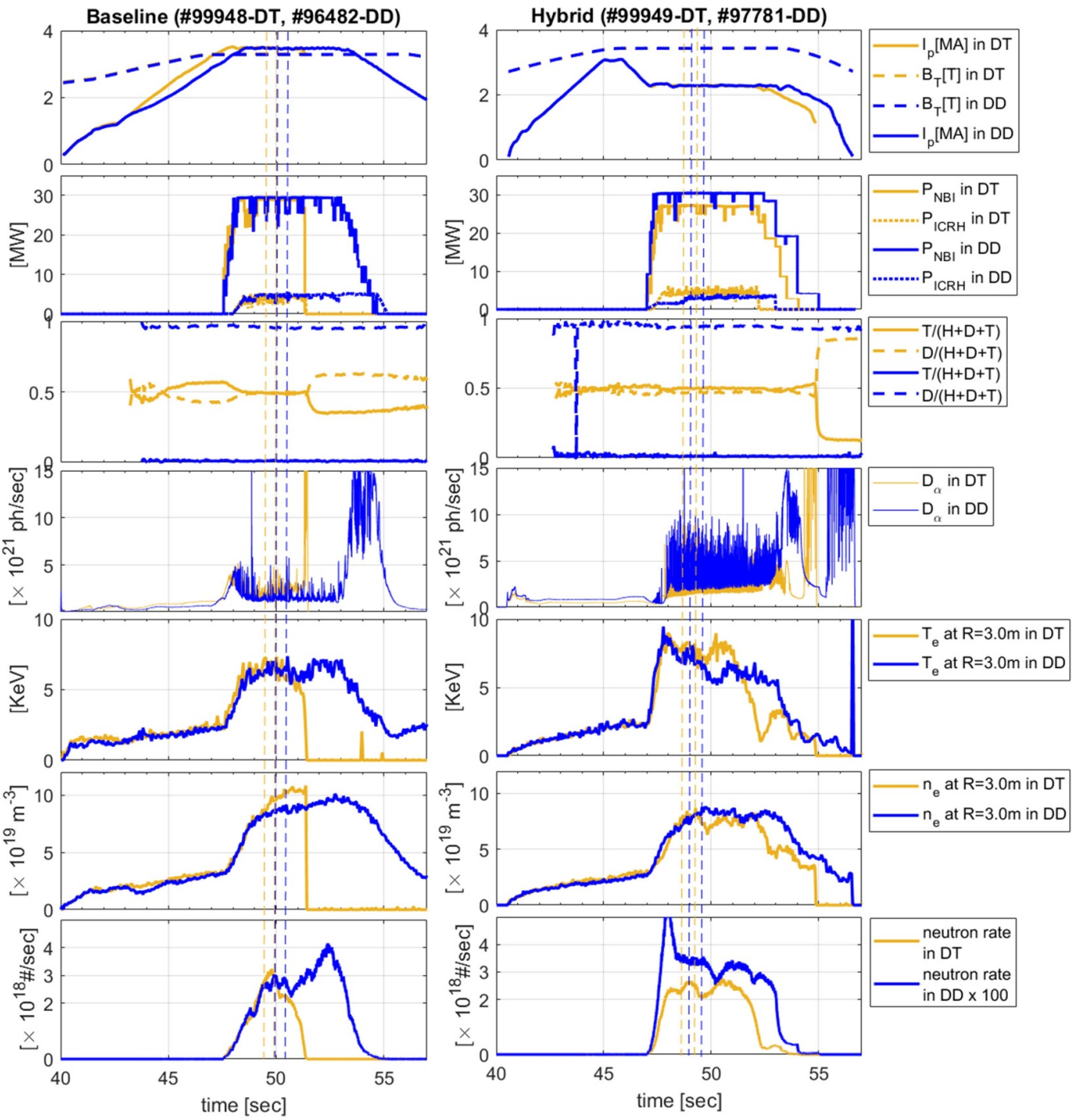

Figure 3. Time traces of reference baseline (50%–50% D–T 99 948 and the counterpart 100% D 96 482) and hybrid discharges (50%–50% D–T 99 949 and 100 % D 97 781). Time windows that were used for predictive modelling have been indicated by vertical dashed lines (gold dashed lines for D–T and blue dashed lines for D) .

with TRANSP, as the heat and particle source profile data in TGYRO are prescribed by interpretive TRANSP data and the same transport model (i.e. TGLF) is used.

To assess the fusion power prediction capability, a standard simulation setting and an identical set of input data were used in all integrated modelling codes (TRANSP-TGLF, JINTRAC-TGLF, JINTRAC-QuaLiKiz, ETS-TGLF, and TGYRO-TGLF), without any posterior adjustment of simulation settings trying to match with experimental data. Table 2 lists the simulation settings, input data, and heating and transport models that were used in all fusion power prediction modelling.

As the quasi-linear transport models are not valid in the pedestal regions where MHD effects are dominant, the measured T_e, T_i, and n_e at $\rho = 0.85$ were used to define the boundary condition in the predictive modelling of the core region (i.e. $\rho \leqslant 0.85$). The boundary condition of T_e and n_e were measured by Thomson scattering system, and T_i was

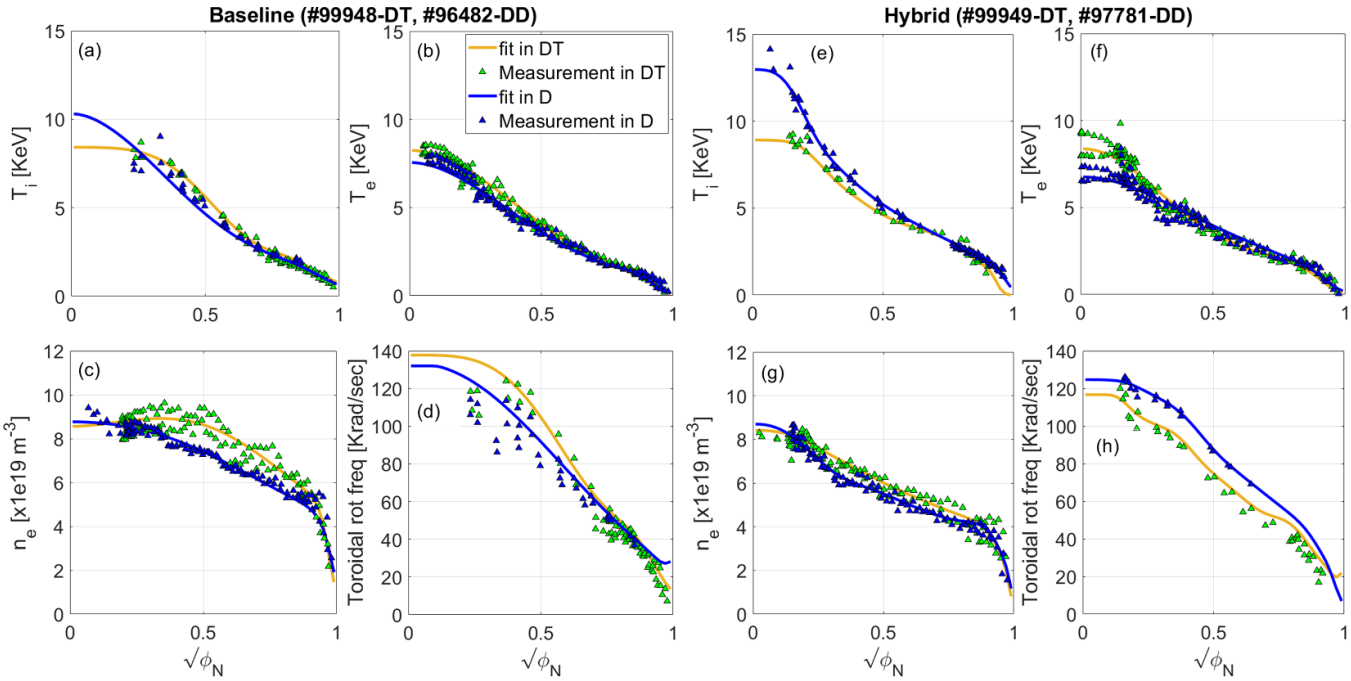

Figure 4. Measured kinetic profiles of the reference baseline (averaged over 49.5–50.0 s in 50%–50% D–T 99 948 and 50.0–50.5 s in the counterpart 100 % D 96 482) and hybrid discharges (averaged over 48.75–49.25 s in 50%–50% D–T 99 949 and 49.0–49.5 s in 100 % D 97 781). T_e and n_e are measured by Thomson scattering and T_i and the rotation frequency are measured by charge exchange radiation spectroscopy.

Table 2. Simulation settings and input data in the modelling for fusion power prediction.

Parameters	Simulation settings
D–T fusion power	Predicted
T_i, n_i, T_e, and n_e for $\rho \leqslant 0.85$	Predicted
T_i at $\rho = 0.85$	Prescribed by charge exchange recombination spectroscopy data
T_e and n_e at $\rho = 0.85$	Prescribed by high resolution Thomson scattering data
Ratio of n_D and n_T for $0 \leqslant \rho \leqslant 0.85$	Prescribed in TRANSP-TGLF by interpretive TRANSP with high resolution H,D,T-alpha spectroscopy data + NBI modelling. Predicted in JINTRAC and ETS by transport models
Rotation frequency for $0 \leqslant \rho \leqslant 0.85$	Prescribed by charge exchange recombination spectroscopy data
Impurity content	Prescribed by interpretive TRANSP data i.e. measured n_e, Zeff data by Bramsstrahlung radiation measurement, and assumption of Be (1% of n_i) and Ni (calculated with quasi-neutrality)
Radiated power density profile	Prescribed by reconstructed Bolometry data
Equilibrium	Calculated with internal Grad–Shafranov solvers
q profile	Calculated with internal poloidal field diffusion equation solvers
NBI heating and particle source	Modelled with NUBEAM in TRANSP, PENCIL in JINTRAC, and ASCOT in ETS
Particle source by gas fuelling and recycling at the wall	Modelled with FRANTIC in TRANSP. Prescribed with TRANSP data in ETS. Not specified in JINTRAC.
ICRF heating	Modelled with TORIC-FPP in TRANSP, PION in JINTRAC, and CYRANO-FOPLA in ETS
Beam-RF synergy	Modelled with each heating model
Neoclassical transport	Modelled with NCLASS
Turbulent transport	Modelled with TGLF(SAT2) or QualiKiZ

measured by charge exchange recombination spectroscopy. Rotation frequency of the main ions can affect the fusion power calculation, as it could change the confinement by reducing turbulence levels and upshifting the ITG threshold of R/L_{Ti} [32]. However, compared to the reasonable maturity of the prediction capability for energy and particle fluxes in the present quasi-linear transport models, the momentum transport prediction is not reliable enough to use. For this reason, whole rotation frequency profiles were prescribed by the profiles measured with charge exchange recombination spectroscopy.

Impurity contents dilute the main fuel ions, and could reduce the fusion power. $Z_{\rm eff}$ measured by Bremsstrahlung radiation diagnostics was given to the interpretive TRANSP modelling, and the content of metallic impurities (i.e. typically assuming 1% beryllium and adjusting the nickel content) were calculated to be consistent with the measured n_e profiles and the quasi-neutrality. The calculated impurity contents were used in the predictive modelling codes. Radiation profiles could affect the electron energy balance, and thereby T_e profile prediction. The radiation profile data was produced by the Bolometry reconstruction, and was prescribed in the predictive modelling.

The D and T fuel mixture ratio could also affect the fusion power calculation. The D–T fuel mixture ratio has been measured using high resolution H,D,T-alpha spectroscopy data in the sub-divertor region. As this is a peripheral measurement, the core D–T fuel mixture should be extrapolated taking into account the impurity and beam dilution. The beam dilution correction requires iterative interpretive TRANSP runs as it requires the beam ion density calculated from a converged slowdown solution. In the first TRANSP run, the core D–T ratio is calculated using a prescribed beam dilution profile, assuming a beam concentration of $\sim 5\%$ with respect to n_e. In the subsequent D–T composition extrapolation, the beam ion density profile calculated by the previous TRANSP run is used in the subsequent D–T composition extrapolation until the extrapolated value converges. It was found that the calculated core value of the D–T concentration was in close agreement with the measured value at the edge region [26], as also predicted by the much shorter relaxation time of the individual isotope ion density profile than the total ion density profile in the nonlinear gyrokinetic simulation of particle transport in multi-isotope plasmas [33]. The ratio of D and T ions calculated from the interpretive TRANSP was used in predictive modelling with TRANSP-TGLF which solves the electron particle balance and the D or T ratio should be prescribed. On the other hand, the D–T mixture ratio in JINTRAC and ETS was calculated with the transport models as they solve the ion particle balances for individual ion species.

The equilibrium and q profiles were calculated with the internal Grad–Shafranov solver and the poloidal field diffusion equation solver in each predictive modelling code.

Modelling of NBI and ICRF heating is crucial for fusion power calculations. NBI heating not only affects T_i profile thereby determining the thermal neutron rate, but also directly produces the beam-thermal neutrons. ICRF heating also affects T_i profile, and it could also accelerate the NBI fast ions (known as the beam-RF synergy), thereby increasing the beam-thermal neutron rate. TRANSP, JINTRAC, and ETS have their own heating models, and brief descriptions of the heating models are provided in the following section. The heating models in each code were used in all simulations, except the JINTRAC-QuaLiKiz simulations for hybrid discharges (D #97 781 and D–T #99 949) due to an unexpected numerical error. In the two exceptional cases, the heat source profiles were prescribed by the calculated values in JINTRAC-TGLF runs i.e. PENCIL/PION.

The particle sources are dominated by the deposition of neutral beams, and they are calculated by the NBI models in each code. Although the pedestal density and temperature were prescribed in the modelling, neutral transport from the wall and atomic reactions (i.e. particle sources near the pedestal) were also calculated by FRANTIC [34] in TRANSP. The number of neutral particles crossing the separatrix is defined by the sum of the gas fuelling data and the recycled neutrals, estimated from the measured edge D_α. In ETS-TGLF, the particle source from the wall is prescribed by the same data in TRANSP-TGLF. In JINTRAC-TGLF and JINTRAC-QuaLiKiz, the particle source from the wall was not specified as the JINTRAC modelling results are not affected when the pedestal density and temperature are prescribed.

3.2.2. Heating models

(i) TRANSP

NBI heating and particle deposition in TRANSP are modelled with NUBEAM, which uses the Monte-Carlo method [23, 24]. About $10\,000 - 30\,000$ Monte-Carlo particles are tracked to model the NBI fast ions, and multiplying weighting factor to the Monte-Carlo particles the distribution of fast ions are simulated. The ionization of beam neutrals is calculated by the mean free path of the atomic reactions of the neutral beams such as charge exchange with thermal ions and impact ionization by thermal ions or electrons. Once beam neutrals are ionized in the plasma, the guiding centre orbit equations are integrated during the slowing down process to calculate where energy and thermalized ions are deposited in the plasma. Integrating the guiding centre orbit equation and applying the displacement in velocity space in each time step, the distribution of fast ions is calculated as a function of position, energy, and pitch angle. NBI heating to electrons and ions, averaged over the flux surfaces, are used in the electron and ion energy balances in TRANSP.

The principal RF wave solver for TRANSP is TORIC [35]. TORIC is coupled to a bounce averaging Fokker–Planck solver, FPP [36], which uses up/down asymmetric equilibria, and computes the phase space distribution of the RF minority ion e.g. H or He-3. The energetic ion distribution function from FPP is used to compute

the collisional transfer to bulk ions and electrons and it also provides an effective tail temperature of the RF minorities that is then used iteratively as a bi-Maxwellian distribution in the TORIC solver. In addition, absorption by electrons, bulk and fast ions can be assessed directly from the wave solver by means of calculating single pass absorption coefficients by each specie from the anti-Hermitian part of dielectric tensor.

To calculate the RF wave power absorption by the NBI fast ions i.e. beam ions and alphas, the Monte Carlo quasi-linear RF kick operator [37, 38] was implemented in NUBEAM and used in all TRANSP runs in this paper. TORIC provides information about the RF electric field components and perpendicular wave vector for each toroidal mode. The RF resonance condition for a given harmonic is then used to calculate the magnetic moment and energy of the particles satisfying the resonant condition. Every time fast ion passes through resonance layer it receives a kick in the magnetic moment space. The magnitude of the kick is derived from the quasi-linear theory, while the stochastic nature of the wave–particle interaction is simulated by adopting the Monte-Carlo approach and the randomness of the phase along the gyro-orbit when the resonance is crossed.

(ii) JINTRAC
PION is the RF heating model in JINTRAC. It solves the power absorption and the pitch angle averaged Fokker–Planck velocity distribution function of resonating ions in a self-consistent way using simplified models [39]. PION is the main heating code installed in the JET data infrastructure which has been validated against many JET experiments. The input data necessary to run the PION code is obtained from the JET experimental database, which provides the necessary information to simulate each discharge. All the input from the JET-database is time evolving, such as the equilibrium, antenna wave frequency, minority concentration and plasma parameters. Therefore, PION provides calculations that evolve in time according to the plasma discharge evolution. Data read by PION is stored for different time points; thus, simulations show the evolution in time of absorption profiles and distribution of velocities of resonant ions for the discharge. As a means to account for NBI heating, the PENCIL code is used [40]. PENCIL computes the beam sources, which are then used as source terms for PION's Fokker–Planck distribution. This allows PION to include ICRH+NBI synergies [41, 42] which is a crucial aspect to consider when trying to optimize scenarios.

(iii) ETS
ASCOT [43] is an orbit-following Monte-Carlo code for solving the Fokker–Planck equation of minority species in tokamaks, e.g. fast ion populations. Within the ETS framework, ASCOT is used as a model for NBI together with BBNBI [44]. ASCOT utilizes a similar set of physics as NUBEAM, integrating the Monte Carlo representation of the neutral beam particle population from initial ionization to thermalization with realistic geometry of the beam particle source. For medium to large conventional tokamaks, such as JET, orbits are followed in guiding-centre space, rather than using full gyro-orbit following.

ICRF heating in ETS is modelled with CYRANO [45]-StixReDis [46]-FoPla. CYRANO is a 2D wave solver accounting for up to second order finite Larmor radius corrections and hence it allows to describe electron ($N = 0$) Landau and transit time magnetic pumping) damping as well as cyclotron damping at the fundamental cyclotron frequency ($N = 1$) and at the second cyclotron harmonic ($N = 2$). The resonance condition pinpointing where the wave-particle energy transfer takes place is $\omega = N\omega_c + kv$ where ω is the wave frequency at the antenna and ω_c is the cyclotron frequency while k and v are the wave vector and particle velocity components along the static magnetic field. StixReDist is a 1D Fokker–Planck equation solver for non-beam populations. Beam populations are calculated with FoPla, which is another 1D Fokker–Planck equation solver, traditionally solved using finite elements. Both FoPla and StixReDist are 1D, and their calculation is fast. However, they are missing trapping effects and effects of anisotropy. Both have the non-linear collision operator so they allow minorities as well as majorities to be modelled. In the ETS modelling of this manuscript, Fokker–Planck equations are solved for all ions where the Coulomb collisional interaction between ion species is consistently calculated.

3.2.3. Turbulent transport models. In large aspect ratio tokamaks including JET, core plasma heat and particle transport is mainly driven by gyro-radius scale micro-instabilities such as the ion temperature gradient mode (ITG), trapped electron mode, and electron temperature gradient mode (ETG). The saturated turbulence level and transport fluxes can be calculated by local flux tube non-linear gyrokinetic simulations such as CGYRO [47] or GENE [48], but this computation is impractically expensive to couple with an integrated modelling code that must cover a large radial extent and long pulse times with consistent heat and particle source calculations.

A quasi-linear transport model is a theory-based reduced model, which is fast enough to be used in predictive integrated modelling. The quasi-linear approximation assumes the turbulence is weak enough that the phase shifts which cause turbulent fluxes are dominated by the most unstable linear eigenmodes [49]. Quasi-linear models usually solve a system of linearized fluid equations describing micro-instabilities, and compute eigenvalues (growth rates and real frequencies) and eigenvectors (phase relations between fluctuating quantities) of the unstable linear eigenmodes. The saturated levels of fluctuating quantities is estimated with a saturation model. Multiplying the quasi-linear weights (linear phase shifts) by the saturation model summed over a poloidal wavenumber spectrum of modes gives the radial turbulent particle, momentum and heat fluxes. The flux surface averaged turbulent transport fluxes are added to the neoclassical collisional fluxes in the particle and energy balance equations. In the predictive integrated modelling in this paper, two main-stream quasi-linear models were used: TGLF and QuaLiKiz.

(i) TGLF
The TGLF model [50] is a quasi-linear turbulent transport model, that solves linearized gyro-fluid equations including the kinetic curvature drift and Landau damping resonances and finite Larmor radius effects [51]. TGLF treats the passing and trapped species in a uniform way with the same system of moment equations for each species giving numerical simplification as well as an extended domain of validity in species and mode number space. TGLF consists of 15 velocity moment equations and a variable number of poloidal ballooning angle basis functions, and plasma species. Several improvements were made to TGLF in order to accurately cover the special physics requirements of the JET-DTE2 discharges. A new version of the saturation model (SAT2 [52]) was developed motivated by the failure of TGLF to reproduce the measured ion energy flux stiffness of JET discharges. SAT2 fits the 3D spectrum (poloidal angle θ, radial wavenumber k_x and poloidal wavenumber k_y) of the saturated potential fluctuations from a database of CGYRO turbulence simulations. The mixture of hydrogenic and impurity species in JET DTE2 discharges required changes to the choice of k_y spectrum used in TGLF. The TGLF equations are valid in the limit of low toroidal rotation velocity relative to the species thermal velocity. In order to avoid violating this limit for metal impurities the toroidal rotation effects, except rotation gradient, were turned off. The switch settings used for the JET DTE2 predictive modelling with TGLF are listed in table 5 in appendix B.

(ii) QuaLiKiz
QuaLiKiz [53, 54] is a quasilinear gyrokinetic code which calculates the turbulent transport. It is kinetic and electrostatic, and thus complementary to the fluid, electromagnetic TGLF. A computational speed sufficient to be used in integrated modelling is reached thanks to a series of assumptions, such as Gaussian eigenfunctions, strongly ballooned modes and a simple *s*-alpha geometry [55]. The collisions are included through a Krook-like operator for trapped electrons. In recent work, the collisional operator was improved through a comparison with GENE [56].

A saturation rule inspired by the nonlinear saturation mechanisms are used to calculate the nonlinear fluxes. The calculations include a form factor, which vanishes at small and large poloidal wavenumber k_y, and two coefficients obtained by a fit to nonlinear simulations, one for ITG and one for ETG scales. An ad-hoc prefactor is included to extend the accuracy to low magnetic shear cases. The lower contribution of the ETG scales, recently discovered during nonlinear studies at JET [57], is included through a multiplier in JINTRAC since not already implemented in the version of QuaLiKiz used in this work.

Extensive validation has been performed on the quasilinear growth rates and frequencies [54, 58], quasilinear cross-phases [59] and nonlinear fluxes [60, 61]. The switch settings used for the predictive modelling with QuaLiKiz are listed in table 6 in appendix C.

3.3. D–T fusion power prediction

3.3.1. Comparison of predicted fusion power. Figures 5(*a*), (*c*), (*e*) and (*g*) compare the time traces of fusion power measured (in black solid lines), calculated in the interpretive TRANSP runs (in black dashed lines), and calculated in the predictive modelling (in coloured solid lines) in the time windows defined in figure 3. As was statistically seen in figure 1, the fusion reaction rate in the interpretive TRANSP runs are very close to the measured values in all cases. This confirms that the main differences of the D–T fusion power calculated in predictive modelling to the measured values result from the differences of the predicted kinetic profiles to the measured profiles. It is worth noting that the magnitude order of predicted fusion power is consistent in the baseline D–T and the counterpart D discharges (i.e. JINTRAC-TGLF, TRANSP-TGLF, ETS-TGLF, and JINTRAC-QuaLiKiz in decreasing order). The same trend is also observed in the hybrid D–T and counterpart D discharges, except one case (TRANSP-TGLF $\leqslant$ ETS-TGLF in 97 781). As will be discussed more in detail in section 3.3.2, this is because the quality of the kinetic profile prediction in the D–T and the counterpart D discharges are similar. When a lower predicted kinetic profile is seen in the D–T discharge, the same feature is also observed in the modelling results of the counterpart D discharge.

The accuracy of D–T fusion power prediction in each code is indicated by normalizing the calculated values to the measured values in figures 5(*b*) and (*f*). In 99 948 (Baseline, D–T) the normalized predicted fusion powers are 65%–96% (i.e. 83% in TRANSP-TGLF, 96% in JINTRAC-TGLF, 65% in JINTRAC-QLK, and 72% in ETS-TGLF), while in 99 949 (Hybrid, D–T) the normalized predicted fusion powers are 81%–97% (i.e. 90% in TRANSP-TGLF, 97% in JINTRAC-TGLF, and 81% in ETS-TGLF).

The normalized neutron rates in the predictive modelling of the counterpart D discharges are shown in figures 5(*d*) and (*h*). It is important to note that the normalized D–T fusion power are similar to the normalized neutron rate in the counterpart D discharges. This is more pronounced in the baseline discharges than in the hybrid discharges, as the contribution of thermonuclear fusion reactions is larger in the baseline discharges. The similarity of the normalized fusion reaction rate between the D–T and the counterpart D discharges was achieved due to the fact that the quality of the kinetic profile prediction in the D–T discharges is maintained in the counterpart D discharges. This implies that the accuracy level of D–T fusion power prediction in the D–T discharges could be *a priori* estimated by the predictive modelling of the counterpart D discharges, which would take place for operation preparation in advance of D–T experiments.

In interpretive TRANSP, the ratio of thermal D–T fusion power to the total power is about 59% and 36% for 99 948

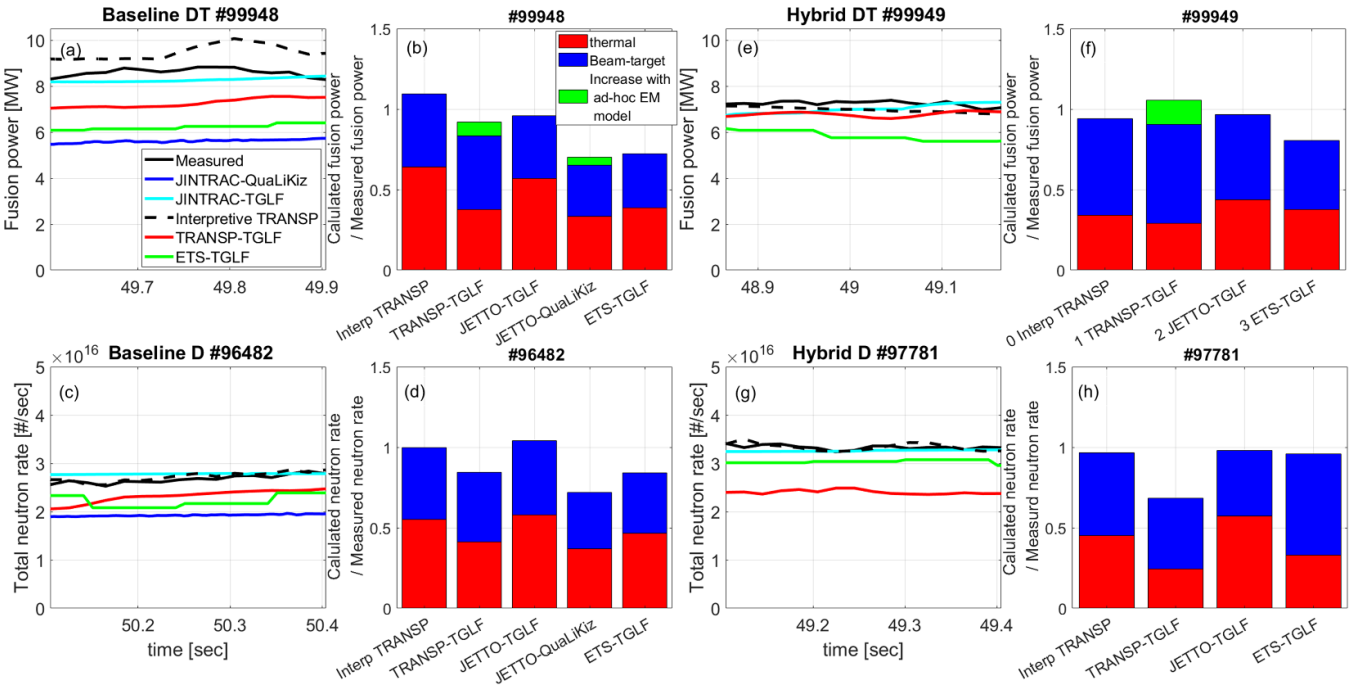

Figure 5. D–T fusion power prediction time traces in (*a*) a reference baseline 50%–50% D–T discharge 99 948 and (*e*) hybrid 50%–50% D–T discharge 99 949. Neutron rate time traces in (*c*) a reference baseline 100% D discharge 96 482 and (*g*) hybrid 100% D discharge 97 781. Normalized neutron rate (*b*) in the baseline 50%–50% D–T discharge 99 948, (*f*) in the hybrid 50%–50% D–T discharge 99 949, (*d*) in the baseline 100% D discharge 96 482, and (*h*) in the hybrid 100% D discharge 97 781. In (*b*) , (*d*) , (*f*) , and (*h*) , the blue and red bars indicate the contribution from the beam-target and the thermal fusion reactions, respectively, in the reference simulation (i.e. without the ad-hoc electromagnetic stabilization model). The gold bars indicate the increase in the thermal neuron rate as predicted by the ad-hoc electromagnetic stabilization model.

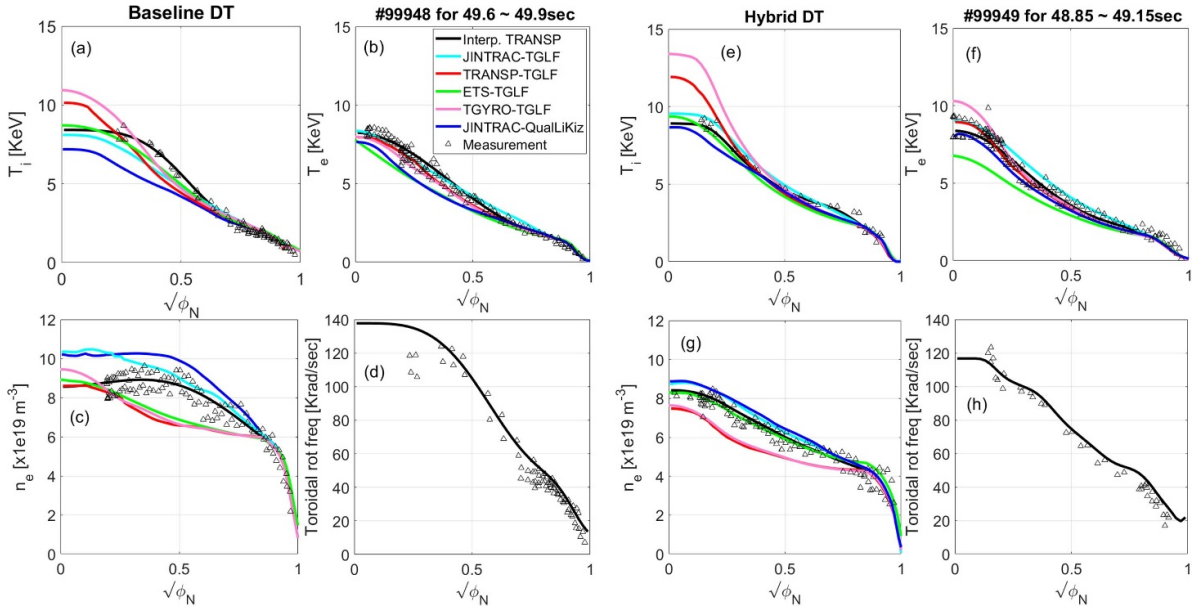

Figure 6. Predicted kinetic profiles in a reference baseline 50%–50% D–T discharge 99 948 and hybrid 50%–50% D–T discharge 99 949.

(Baseline, D–T) and 99 949 (Hybrid, D–T), respectively. The higher thermal D–T fusion power ratio in 99 948 (Baseline, D–T) is due to the higher ion density, which is a typical feature of baseline scenarios operated at high I_p. High ion density directly increases the thermal D–T fusion reaction rate, but reduces the beam-thermal fusion reaction rate. In high ion density plasmas, NBI particles are more deposited near the pedestal region reducing the beam deposition in the core region. The beam particles deposited near the pedestal region have a smaller probability of fusion reaction than those deposited in the core region, as they are likely to be slowed down through collisions with electrons due to the low T_e.

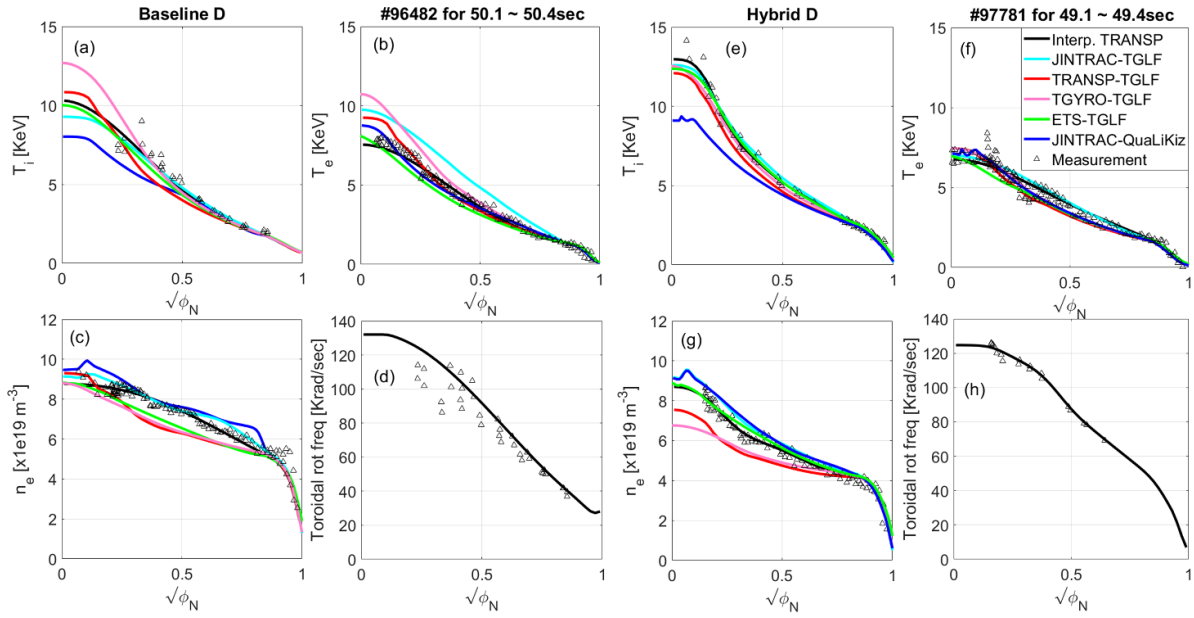

Figure 7. Predicted kinetic profiles in a reference baseline 100% D discharge 96 482 and hybrid 100% D discharge 97 781.

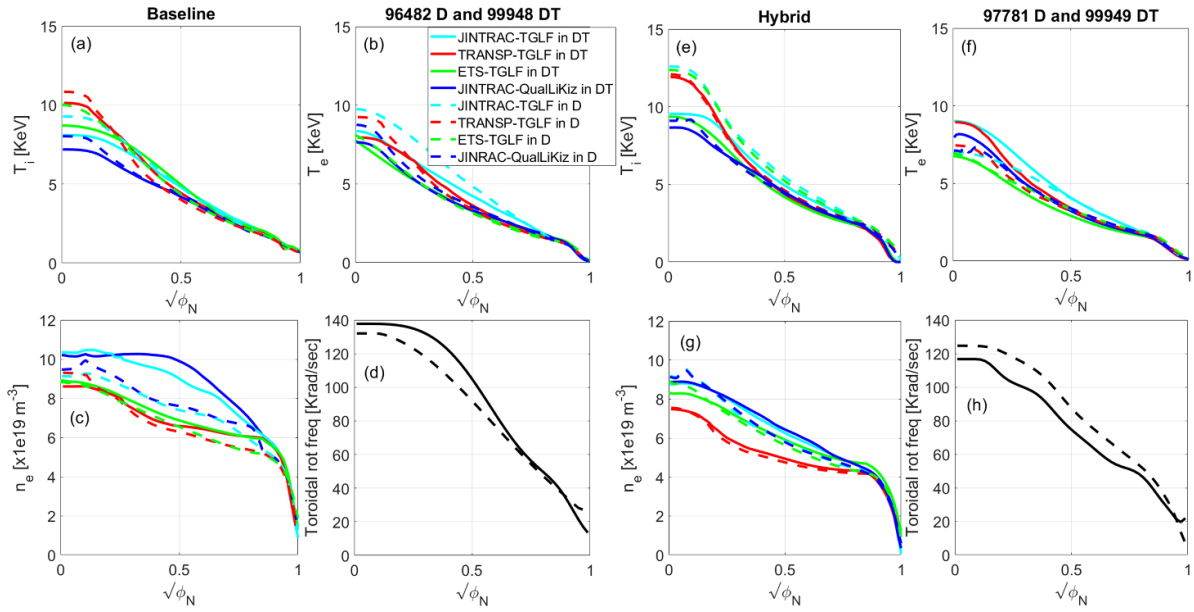

Figure 8. Comparison of the predicted profiles in D and D–T discharges.

3.3.2. Comparison of predicted kinetic profiles. Figures 6 and 7 compare the predicted kinetic profiles with the measured profiles in the D–T and the counterpart D discharges, respectively. Overall, when the kinetic profiles are well predicted in the D–T discharges, they are also well reproduced in the counterpart D discharges. One of the main differences in the measured profiles between the D–T and the counterpart D discharges is n_e profile, which is higher in the D–T discharges (see figure 4). JINTRAC-TGLF and JINTRAC-QuaLiKiz well reproduce the higher n_e profiles in 99 948 (Baseline D–T), and the lower n_e profile in 96 482 (Baseline D) as well. On the other hand, when the kinetic profiles are underpredicted in the D–T discharges, they are also underpredicted in the counterpart D discharges. In 99 948 (Baseline, D–T), n_e profiles are underpredicted with TRANSP-TGLF and ETS-TGLF compared to the measured profile. The similar underprediction of n_e is also observed in 96 482 (Baseline, D). Another example is T_i profile in the baseline discharges. T_i for wide radial window ($\rho = 0 - 0.5$) in 99 948 (Baseline, D–T) is underpredicted with JINTRAC-QuaLiKiz, and the same feature is also seen in 96 482 (Baseline, D). These observations indicate that in the present predictive integrated modelling codes the features of predicted kinetic profiles in D–T discharges appear in the predicted kinetic profiles of the counterpart D discharges as well, and the prediction quality of D–T discharges could be assessed with the predictive modelling quality of the counterpart D

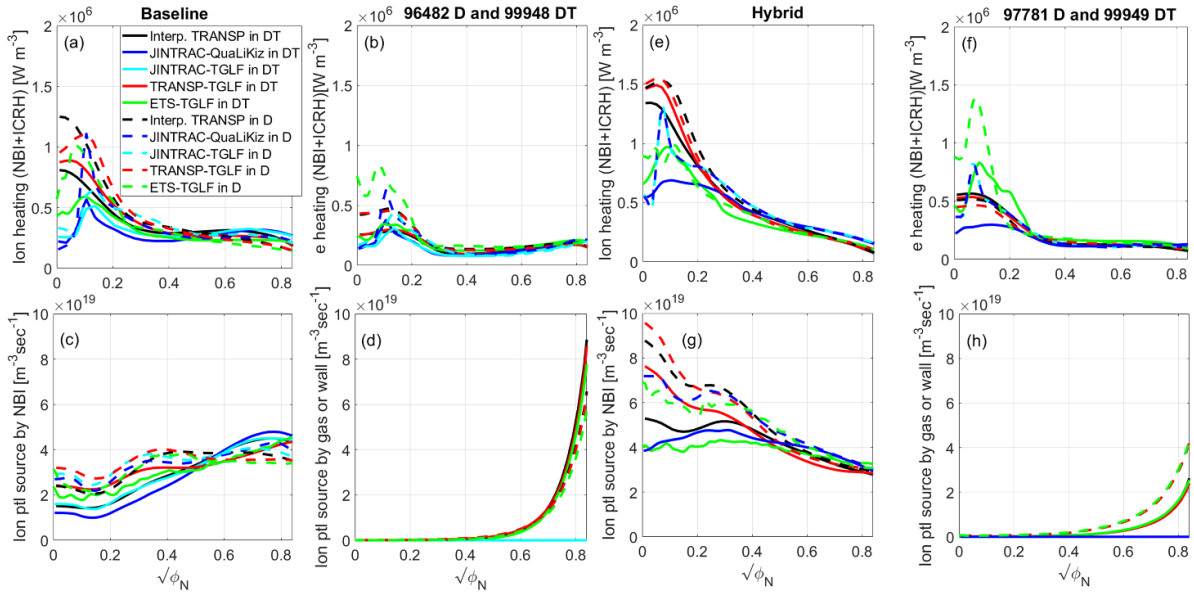

Figure 9. Heat and particle sources in predictive simulations of a reference baseline 50%–50% D–T discharge 99 948 and hybrid 50%–50% D–T discharge 99 949.

discharges, which would take place in preparation of the D–T discharge operation.

Figure 8 directly compares the predicted kinetic profiles between the D–T (solid lines) and D (dashed lines) discharges. Since the identical models and the same simulation settings (other than the different fuel gas mixture and the different boundary condition) were used in the predictive simulation of the D–T and the counterpart D discharges, the differences of predicted kinetic profiles between them can be attributed to the isotope effects in the predictive integrated modelling codes. Most predicted kinetic profiles in TRANSP-TGLF and ETS-TGLF are similar between the D–T and the counterpart D discharge, indicating there is no significant isotope effects in TRANSP-TGLF. On the other hand, JINTRAC-TGLF and JINTRAC-QuaLiKiz have higher n_e profiles predicted for the D–T discharges than that for the counterpart D discharges. This is consistent with what is observed in the measured profiles, implying that the isotope effects on the particle transport resulting from the different fuel gas mixture is well captured in the modelling.

Another feature worth noting in figure 8 is that the core T_i within $\rho < 0.2$ are all lower in the D–T discharges than in the counterpart hybrid D discharges. This could be because D NBI beams have a higher penetration, thus higher core ion heating, as can be seen in figures 9(*a*) and (*e*) .

TGYRO-TGLF has also participated in the collective modelling for code benchmark purpose, as the input data in TGYRO-TGLF was given from the interpretive TRANSP runs. The TGYRO case is different from the other predictive modelling cases. It uses prescribed heat and particle source profiles, while the other codes calculate heating and particle source profiles self-consistently with evolving kinetic profiles. Since there is no modelling of the NBI beam ion slowing-down, the TGYRO-TGLF simulation was not available to calculate the fusion power data. Figures 6 and 7 show that all the predicted kinetic profiles in the TRANSP-TGLF and TGYRO-TGLF simulations are very similar, including even the underpredicted n_e profiles in both discharges. This confirms the consistency between the two codes, including the interface with TGLF.

The calculated fusion power in figure 5 is consistent with the calculated kinetic profiles in figure 6. First of all, figure 6 shows that the calculated kinetic profiles in JINTRAC-TGLF (cyan solid lines) agrees well with the measured data points (triangles) for both 99 948 (Baseline, D–T) and 99 949 (Hybrid, D–T). The calculated fusion power in JINTRAC-TGLF (cyan solid lines) also agrees well with the measured fusion power (black solid lines) for both 99 948 (Baseline, D–T) and 99 949 (Hybrid, D–T) in figure 5. This confirms that D–T fusion power could be closely calculated to the measurement if kinetic profiles are correctly predicted in the present integrated modelling code.

The cases of fusion power underprediction can also be individually explained with the predicted kinetic profiles. In both 99 948 (Baseline, D–T) and 99 949 (Hybrid D–T), TRANSP-TGLF (red solid lines) has significantly lower n_e profiles than the values measured with Thomson scattering diagnostics. This indicates that the predicted ion densities are lower than the actual values in the discharge. On the other hand, the predicted T_i profiles agrees well with the values measured by charge exchange recombination spectroscopy. This confirms that the underprediction of the ion densities in TRANSP-TGLF is the main cause leading to the underprediction of fusion power in both baseline and hybrid D–T discharges. The n_e underprediction issue is further discussed in section 3.4.

ETS-TGLF (green solid lines) has the same reason for the fusion power underprediction in 99 948 (Baseline, D–T). The n_e profile is underpredicted while the predicted T_i profile reasonably well agrees with the measurement. It is worth noting that even the shape of the underpredicted n_e profile is similar

Table 3. Summary of the reasons for the underpredicted fusion power in each case.

Codes	Baseline D–T 99 948	Hybrid D–T 99 949
Interpretive TRANSP	Good P_{fus} prediction (109%)	Good P_{fus} prediction (94%)
JINTRAC-TGLF	Good P_{fus} prediction (96%)	Good P_{fus} prediction (97%)
TRANSP-TGLF	Underpredicted P_{fus} (83%) due to underpredicted n_i	Underpredicted P_{fus} (90%) due to underpredicted n_i
TGYRO-TGLF	Underpredicted n_i	Underpredicted n_i
ETS-TGLF	Underpredicted P_{fus} (72%) due to underpredicted n_i	Underpredicted P_{fus} (81%) due to underpredicted T_e (low beam-thermal fusion)
JINTRAC-QuaLiKiz	Underpredicted P_{fus} (65%) due to underpredicted T_i	Underpredicted T_i

as TRANSP-TGLF. This implies that both cases have the same cause. However, such underprediction of n_e in ETS-TGLF disappears in 99 949 (Hybrid, D–T). ETS-TGLF reproduces n_e and T_i profiles at a good agreement with the measurement in 99 949 (Hybrid, D–T). It is important to note that ETS-TGLF still mildly underpredicts the fusion power despite the good T_i and n_e (hence n_i) prediction. The underpredicted fusion power with ETS-TGLF in the hybrid D–T discharge is attributed to the relatively low beam-thermal fusion reactions. As can be seen in figure 9(*g*) , the NBI particle deposition to the core region in the ETS-TGLF simulation is likely good enough, as indicated by the similar level as the JINTRAC-TGLF, which well predicts the fusion power. However, the predicted T_e profile in ETS-TGLF is much lower than the measured value, and this reduces the beam-thermal fusion reaction rate as the probability of fast ions slowing down by collisions with electrons increases at low T_e.

JINTRAC-QuaLiKiz (blue solid lines) also underpredicts the fusion power in 99 948 (Baseline, D–T), but it has a different reason. The predicted n_e reasonably agrees with the measurement, implying that the ion density is well reproduced. However, T_i profile is lower than the measurement. The underpredicted T_i is also seen in JINTRAC-QuaLiKiz in 99 949 (hybrid D–T). This implies that the ion heat transport in JINTRAC-QuaLiKiz is overcalculated. As can be seen in figures 9(*a*) and (*e*) , the ion heating profiles in JINTRAC-QuaLiKiz are similar to those in JINTRAC-TGLF, which well reproduces the T_i profiles in both discharges. The higher ion heat transport in JINTRAC-QuaLiKiz should be due to the fact that QuaLiKiz is an electrostatic model. This is more discussed in section 3.4.

In summary, the predicted D–T fusion power is well matched with the measured values when the kinetic profiles are correctly given (i.e. interpretive TRANSP) or predicted (i.e. JINTRAC-TGLF). In the other cases, the D–T fusion power is underpredicted due to the underpredicted kinetic profiles. The reasons for the underpredicted fusion power in each case are summarized in table 3, and are discussed in section 3.4.

3.4. Discussion

3.4.1. Candidates for underpredicted kinetic profiles. The underprediction of n_e in TRANSP-TGLF is the main cause for the underpredicted fusion power i.e. 83% in 99 948 (Baseline, D–T) and 90% in 99 949 (Hybrid, D–T). Such an underprediction is not seen in the predicted n_e profiles with JINTRAC-TGLF, despite the absence of the particle sources from the wall recycling or gas fuelling (see figures 9(*d*) and (*h*)). The core particle source profile does not explain the lower n_e either. As can be seen in figures 9(*c*) and (*g*), the particle deposition in the core region is actually higher in TRANSP-TGLF than the ion particle source in JINTRAC-TGLF.

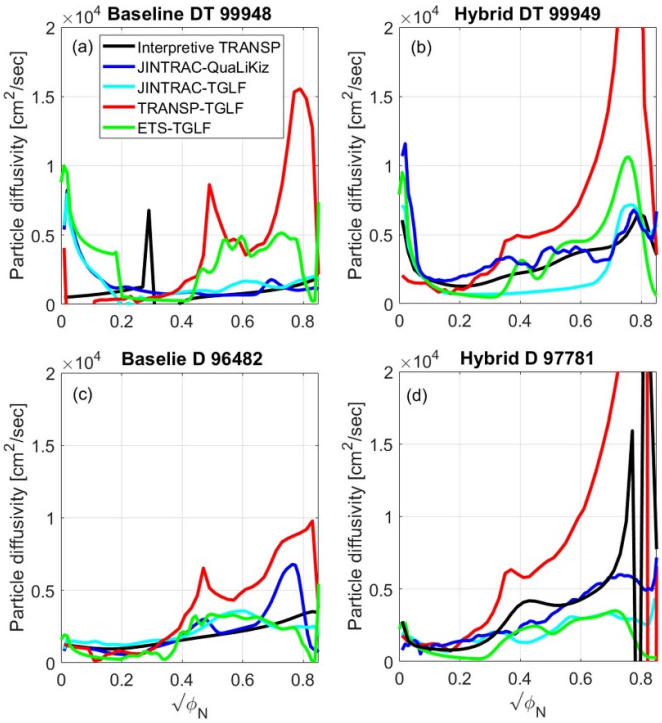

Figure 10. Effective particle diffusivity in (*a*) baseline D–T 99 948, (*b*) hybrid D–T 99 949, (*c*) baseline D 96 482, and (*d*) hybrid D 97 781.

The underprediction of the n_e profiles in TRANSP-TGLF is probably due to the large particle diffusivity. Figure 10 shows that the effective particle diffusivity D, which includes both the particle diffusion resulting from the density gradient and the convection terms, i.e. pinch effects. TRANSP solves the electron particle balance and the ion density is calculated for quasi-neutrality with the prescribed impurity content and D–T ratio. On the other hand, JINTRAC and ETS solve the ion particle

balance equation for D and T ions individually (and the n_e profile is calculated for quasi-neutrality). Thus D in interpretive TRANSP is the *electron* particle diffusivity derived from the prescribed n_e profile. In TRANSP-TGLF, D is also the *electron* particle diffusivity, but calculated by TGLF. In ETS and JINTRAC D is the *ion* particle diffusivity computed by TGLF or QuaLiKiz. Figure 10 shows the D in TRANSP-TGLF are much higher than the D in interpretive TRANSP, especially for $\rho = 0.7 - 0.85$. This reduces the n_e density gradient in $\rho = 0.7 - 0.85$, leading to the n_e underprediction in the core region. The D in JINTRAC-TGLF is much closer to the D in interpretive TRANSP, allowing the predicted n_e profile to be close to the measurement.

Figure 10 shows that the large particle diffusivity in TRANSP-TGLF caused the underprediction of n_e. However, it is not clear why the same quasilinear transport model could produce such large differences in particle diffusivities. ETS-TGLF also has different D profiles, though the differences to D in JINTRAC-TGLF is mild. One of the possible candidates could be the different way particle transport is treated in TRANSP, JINTRAC and ETS. Comparison of the interface of the TGLF in each integrated modelling code should provide a clue. However, further investigation of this issue is not included in this paper, as detailed code benchmarking is beyond the scope of this paper.

Regarding the underprediction of T_i in JINTRAC-QuaLiKiz, one candidate could be the lack of electromagnetic stabilization of the turbulent transport. The electromagnetic stabilization is absent in JINTRAC-QuaLiKiz as QuaLiKiz is an electrostatic model. Furthermore, in the recent JET modelling, it has been reported that electromagnetic effects could suppress the ITG-driven turbulence and the effects could be enhanced by the presence of fast ion pressure gradient [62–64]. The electromagnetic stabilization of the ITG mode by fast ions was not taken into account in the predictive modelling of this paper. Although TGLF is an electromagnetic model, a complete treatment taking into account the fast ions as kinetic species in the electromagnetic calculation is, however, not available in the present version of TGLF. In the current quasi-linear models, while linear effects of fast ion can be captured, the saturation rules do not take into account the more significant impact of nonlinear stabilization by fast ions. Alternatively, [21] reported that a JET discharge was successfully reproduced with an ad-hoc model in QuaLiKiz, with which the ∇T_i input to the quasi-linear transport model is reduced by a factor of the local $p_{\mathrm{thermal}}/p_{\mathrm{total}}$. The ad-hoc model effectively shifts up the threshold value of ∇T_i to trigger the ITG mode, thereby improving the energy and particle confinement in the modelling. The ad-hoc model has also recently been implemented in TRANSP-TGLF. It was found that use of the ad-hoc model increases the thermal D–T fusion power by 9% in TRANSP-TGLF for 99 948, 15% in TRANSP-TGLF for 99 949, and 5% in JINTRAC-QuaLiKiz for 99 948 (indicated by the gold bars in figures 5(*b*) and (*d*)), enabling a closer fusion power reproduction towards the measurement. The improved agreement with the ad-hoc model suggests a possibility that the underpredicted fusion power in the present predictive modelling is partly due to the lack of the electromagnetic stabilization of ITG. This could make more direct impact, in particular, to the JINTRAC-QuaLiKiz modelling where T_i was underpredicted. To confirm this hypothesis and to correctly quantify the fusion power increase, an improved model with more rigorous physics basis is needed.

3.4.2. Uncertainties for ITER D–T fusion power prediction. The baseline D–T operation in ITER is planned to achieve $I_p = 15$ MA, $B_\phi = 5.3$ T, heating power = 50 MW, and fusion power = 500 MW i.e. $Q = 10$. In the ITER plasma, the D–T neutron rate is expected to be about two orders of magnitude higher than in JET D–T discharges. The predictive modelling codes validated in this paper confirm good or moderate fusion power prediction capability for the JET D–T discharges relevant to the ITER conditions, e.g. baseline scenario and ITER-Like wall. As the heating and transport models used are physics-based models, it is expected that the present predictive modelling tools will be valid for ITER D–T prediction, provided that the plasma regime is similar (e.g. ITG-mode dominant transport). However, it should be noted that the following uncertainties are present and need to be addressed.

Figure 5 has shown that the prediction quality of the kinetic profiles and the fusion reaction rate in the D–T discharges and the counterpart D discharges are similar. This should be possible because the alpha heating in the present JET D–T discharges is tiny (see figure 2(*d*)) and the effect on the T_i profiles is negligible. The present alpha heating model is based on the same physics model used for D or T NBI fast ion heating. However, the applicability of the present Monte-Carlo method based model to the alpha heating has not yet been validated against experimental data. If any significantly different physics of alpha heating or transport, such as toroidal Alfven eigenmodes (TAE)-driven alpha ion losses [65], alpha heat and momentum channelling [66], or improved ITG stabilization by alpha particles [67], turns out to be important, the predicted fusion power could be affected, especially for ITER, where the alpha heating should be the dominant heating power. In addition, thermalized alpha particles (i.e. He ashes) could accumulate and dilute the fuel ions. This could significantly reduce the D–T fusion power. The transport of He ash should also be correctly predicted for fusion power prediction in long pulse D–T discharges.

As shown in the previous sections, D–T fusion power prediction is subject to the quality of kinetic profile prediction. In the predictive modelling in this papers, rotation frequency profile, pedestal density and temperature, impurity content were prescribed by experimental data. The prediction of fusion power from core predictive modelling depends on these prescribed parameters, so there will be uncertainties if they are also predicted. In particular, one of the main differences of the D–T discharges compared to the counterpart D discharges is the higher pedestal n_e, which is determined by MHD physics such as ELMs. The sensitivity of D–T fusion power calculation to the prescribed parameters should be quantified to assess the uncertainties resulting from the boundary condition,

and predictive modelling or scaling law of the prescribed parameters should be developed and validated for ITER D–T fusion power prediction.

Gas fuelling could be another source of prediction uncertainty. In the modelling with TRANSP-TGLF and ETS-TGLF in this paper, the neutral particles produced by recycling of the main fuel ions at the wall were estimated as the measured number of edge D alpha photons. It is a rough estimate and has a large uncertainty. Also, the temperature of the neutral particles recycled at the wall or provided by the gas puffing is assumed to be 3 eV, as there is no sophisticated neutral particle modelling available in the present modelling. This temperature could vary, and if it is higher (e.g. due to backscattering energy at the wall), the neutral particle influx into the plasma should increase [68]. It was found that the predicted core n_e profiles near the boundary ($\rho = 0.85$) could be altered by increasing the neutral particle influx, and the effect could also propagate into the core profile. The modification of the core n_e profile by different gas puffing data was also observed in JINTRAC when the pedestal is modelled (i.e. boundary condition at the separatrix) [22, 69]. Improved modelling of the neutral particle sources from the edge region would improve the core profile prediction near the pedestal.

4. Conclusion

D–T fusion power calculated by the interpretive TRANSP runs of 38 D50%–T50% baseline or hybrid discharges in 2021 JET D–T experimental campaign have achieved a high level of agreement with the measured fusion power, of which deviation is less than 20% for all discharges. This indicates the validity of the D–T fusion reaction cross section data, measured impurity content, and the measured kinetic profiles in the 2021 JET D–T experiment data, and also the validity of the NBI and ICRF models used for the beam-thermal neutron rate. The good statistical agreement confirms that we have the capability to accurately calculate the D–T fusion power if correct kinetic profiles are known.

Core predictive integrated modelling has been performed for the two ITER-relevant D–T discharges in the 2021 JET D–T experimental campaign i.e. high performance stationary D–T baseline and hybrid discharges operated with the ITER-Like full metallic wall. Since each integrated modelling code has different equilibrium, heating, and transport models, to assess uncertainties arising from the choice of the modelling code, the standard simulation settings and experimental input data were identically used in the integrated modelling codes (TRANSP, JINTRAC, and ETS) coupled to the mainstream quasi-linear turbulent transport models (TGLF or QuaLiKiz). The accuracy levels of predicted D–T fusion power normalized with the measured fusion power were found as 65%–96% for the baseline (i.e. 83% in TRANSP-TGLF, 96% in JINTRAC-TGLF, 65% in JINTRAC-QuaLiKiz, and 72% in ETS-TGLF) and 81%–97% for the hybrid discharge (i.e. 90% in TRANSP-TGLF, 97% in JINTRAC-TGLF, and 81% in ETS-TGLF). Based on the high accuracy of the normalized fusion power calculated in the interpretive TRANSP runs i.e. 109% in baseline and 94% in hybrid, any larger deviation in the predicted D–T fusion power is most probably due to errors in the predicted kinetic profiles. The consistency between the deviated predicted kinetic profiles and the lower predicted D–T fusion power compared to measured fusion power has been cross-checked in all predictive simulations. The underpredicted kinetic profiles that lead to the lower fusion power prediction have been identified in each integrated modelling code, and possible reasons for the underprediction of kinetic profiles were discussed.

The normalized neutron rate in the predictive simulations of the counterpart D discharges, where the key engineering parameters are similar to the D–T discharges, are similar to the normalized D–T fusion power. This is due to the fact that the quality of the predicted kinetic profiles in the D–T discharges are maintained in the counterpart D discharges. It implies that the D–T fusion power prediction credibility could be assessed by the reproducibility of preparatory D discharges, which would be produced in advance of D–T experiments.

The uncertainties of the predicted profiles are discussed and future work is suggested to reduce the prediction uncertainties. In the core predictive modelling in this paper, the following input data from experimental measurements were used: boundary condition of T_i , T_e and n_e , total rotation frequency profile, impurity content and radiated energy loss profile. For ITER D–T prediction they should be predicted with validated physics models in an integrated modelling workflow. In addition, in the burning plasma state of ITER D–T, the physics of energetic alpha particles, such as TAE-driven alpha ion losses, alpha channelling or improved electromagnetic ITG stabilization by alpha particles, could make significant differences compared to D discharges. Transport of thermalized alpha particles (i.e. helium ash) is also important in long pulse DT discharges, as they could dilute the fuel ions, thereby reducing fusion power. The development and validation of a more complete model of alpha particle heating and transport would improve the ITER D–T prediction capability.

Acknowledgments

This work has been carried out within the framework of the EUROfusion Consortium, funded by the European Union via the Euratom Research and Training Programme (Grant Agreement No 101052200 - EUROfusion) and from the EPSRC (Grant Number EP/W006839/1). The BSC part of this work is grateful for the support received from the Departament de Recerca i Universitats de la Generalitat de Catalunya via the Research Group Fusion Group with code: 2021 SGR 00908. To obtain further information on the data and models underlying this paper please contact PublicationsManager@ukaea.uk. Views and opinions expressed are however those of the author(s) only and do not necessarily reflect those of the European Union or the European Commission. Neither the European Union nor the European Commission can be held responsible for them.

Appendix A. D–T discharges for interpretive TRANSP runs

Table 4. Database of D–T neuron rates calculated with interpretive TRANSP for baseline and hybrid discharges in 2021 JET D–T experimental campaign.

Shot number	Operation scenario	Time window (sec)	Measured D–T neutron rate (#/sec)	Calculated D–T neutron rate (#/sec)	I_p [MA]	B_T [T]	P_{NBI} [MW]	P_{ICRF} [MW]
99 512	baseline	48.6–49.1	$1.24 \times 10^{+18}$	$1.46 \times 10^{+18}$	3.0	2.8	26.4	1.6
99 513	baseline	48.5–49.5	$1.19 \times 10^{+18}$	$1.27 \times 10^{+18}$	3.0	2.8	24.2	1.8
99 520	baseline	49.0–50.0	$1.18 \times 10^{+18}$	$1.25 \times 10^{+18}$	3.5	3.3	23.0	2.7
99 523	baseline	49.0–50.0	$1.38 \times 10^{+18}$	$1.55 \times 10^{+18}$	3.5	3.3	24.5	2.5
99 797	baseline	49.0–50.0	$2.03 \times 10^{+18}$	$2.41 \times 10^{+18}$	3.5	3.3	25.9	3.8
99 799	baseline	49.0–50.0	$2.37 \times 10^{+18}$	$2.44 \times 10^{+18}$	3.5	3.3	26.29	3.9
99 863	baseline	49.0–50.0	$2.83 \times 10^{+18}$	$2.99 \times 10^{+18}$	3.5	3.3	28.4	3.4
99 891	baseline	48.8–49.9	$9.68 \times 10^{+17}$	$1.20 \times 10^{+18}$	3.0	2.8	27.0	2.5
99 915	baseline	49.0–50.0	$2.50 \times 10^{+18}$	$2.73 \times 10^{+18}$	3.5	3.3	26.6	3.5
99 916	baseline	49.4–50.4	$2.22 \times 10^{+18}$	$2.50 \times 10^{+18}$	3.5	3.3	27.9	3.7
99 943	baseline	49.0–50.0	$2.55 \times 10^{+18}$	$2.69 \times 10^{+18}$	3.5	3.3	28.7	3.7
99 948	baseline	49.0–50.0	$2.71 \times 10^{+18}$	$2.86 \times 10^{+18}$	3.5	3.3	28.7	3.5
99 449	hybrid	47.5–48.5	$2.42 \times 10^{+18}$	$2.74 \times 10^{+18}$	2.3	3.4	26.0	1.5
99 455	hybrid	47.5–48.5	$1.81 \times 10^{+18}$	$1.89 \times 10^{+18}$	2.3	3.4	24.2	1.5
99 527	hybrid	47.5–48.5	$2.53 \times 10^{+18}$	$2.70 \times 10^{+18}$	2.3	3.4	24.5	1.5
99 528	hybrid	47.5–48.5	$2.27 \times 10^{+18}$	$2.27 \times 10^{+18}$	2.3	3.4	22.4	1.2
99 541	hybrid	48.5–49.5	$1.46 \times 10^{+18}$	$1.46 \times 10^{+18}$	2.3	3.4	24.3	4.0
99 542	hybrid	47.5–48.5	$1.84 \times 10^{+18}$	$1.59 \times 10^{+18}$	2.3	3.4	20.1	3.3
99 544	hybrid	47.5–48.5	$1.42 \times 10^{+18}$	$1.55 \times 10^{+18}$	2.3	3.4	19.7	2.5
99 594	hybrid	49.0–50.0	$2.09 \times 10^{+18}$	$2.29 \times 10^{+18}$	2.3	3.4	26.5	3.9
99 595	hybrid	49.0–50.0	$1.58 \times 10^{+18}$	$1.75 \times 10^{+18}$	2.3	3.4	26.2	4.0
99 596	hybrid	49.0–50.0	$2.13 \times 10^{+18}$	$2.10 \times 10^{+18}$	2.3	3.4	26.0	4.7
99 760	hybrid	48.0–49.0	$2.13 \times 10^{+18}$	$2.02 \times 10^{+18}$	2.3	3.4	24.4	3.8
99 761	hybrid	48.0–49.0	$2.29 \times 10^{+18}$	$2.19 \times 10^{+18}$	2.3	3.4	25.7	4.1
99 767	hybrid	48.0–49.0	$2.07 \times 10^{+18}$	$2.13 \times 10^{+18}$	2.3	3.4	24.1	4.1
99 866	hybrid	48.0–49.0	$2.62 \times 10^{+18}$	$3.03 \times 10^{+18}$	2.3	3.4	24.3	3.9
99 867	hybrid	49.0–50.0	$2.72 \times 10^{+18}$	$3.04 \times 10^{+18}$	2.3	3.4	27.1	4.3
99 868	hybrid	48.0–49.0	$2.51 \times 10^{+18}$	$2.55 \times 10^{+18}$	2.3	3.4	25.1	3.8
99 869	hybrid	49.0–50.0	$2.84 \times 10^{+18}$	$2.88 \times 10^{+18}$	2.3	3.4	25.8	4.1
99 887	hybrid	49.0–50.0	$3.37 \times 10^{+18}$	$3.39 \times 10^{+18}$	2.3	3.4	27.8	4.2
99 908	hybrid	49.0–50.0	$3.08 \times 10^{+18}$	$2.90 \times 10^{+18}$	2.3	3.4	26.3	3.7
99 910	hybrid	49.0–50.0	$3.44 \times 10^{+18}$	$3.43 \times 10^{+18}$	2.3	3.4	27.8	4.3
99 912	hybrid	49.0–50.0	$3.75 \times 10^{+18}$	$3.75 \times 10^{+18}$	2.3	3.4	29.1	4.2
99 914	hybrid	49.0–50.0	$2.71 \times 10^{+18}$	$2.68 \times 10^{+18}$	2.3	3.4	25.4	3.6
99 949	hybrid	49.0–50.0	$2.29 \times 10^{+18}$	$2.43 \times 10^{+18}$	2.3	3.4	26.5	4.3
99 950	hybrid	49.0–50.0	$3.46 \times 10^{+18}$	$3.30 \times 10^{+18}$	2.3	3.4	28.0	4.3
99 951	hybrid	48.0–49.0	$3.14 \times 10^{+18}$	$3.15 \times 10^{+18}$	2.3	3.4	26.7	4.5
99 953	hybrid	49.0–50.0	$2.48 \times 10^{+18}$	$2.65 \times 10^{+18}$	2.3	3.4	24.9	4.6

Table 4 indicates the shot numbers, the time window, the measured neutron rate, and the neutron rate with the interpretive TRANSP in the $50\% - 50\%$ D–T discharges in figure 1.

Appendix B. TGLF settings

Table 5. TGLF switch setting used for the predictive simulation of JET D–T baseline and hybrid discharges in figure 6.

Switch	Definition	Setting in TRANSP	Setting in JINTRAC	Setting in ETS
NS	# of kinetic species	4 (e, D, T, effective impurity)	4 (e, D, T, effective impurity)	6 (e, D, T, H minority, two impurities)
GEOMETRY _FLAG_MODEL	1 is for Miller geometry	1	1	1
USE_BPER	Include perpendicular magnetic fluctuations i.e. $\delta A_{\|\|}$	T	T	T
USE_BPAR	Include parallel magnetic fluctuations i.e. $\delta B_{\|\|}$	F	F	F
SAT_RULE	saturation rule	2	2	2
KYGRID_MODEL	4 is to use standard spectrum for transport model and start making at a lower ky	4	4	4
NMODES	# of stored modes	6	6	8
NBASIS_MIN	minimum number of parallel basis function	2	2	2
NBASIS_MAX	maximum number of parallel basis function	6	6	6
NKY	# of poloidal modes in the high-k spectrum	19	19	19
ALPHA_MACH	multiplies parallel velocity for all species	0	0	0
APLHA_E	multiplies ExB velocity shear for spectral shift model	1	1	1
ALPHA_QUENCH	0 is to use new spectral shift model	0	0	0
FILTER	sets threshold for frequency/drift frequency to filter out non-driftwave instabilities	2.0	2.0	2.0
USE_AVE_ION_GRID	to make the ky-grid independent of the order of the ions but computing a charge average reference ρ_i to use in the ky-grid generation	T	T	T

The TGLF source code was obtained from https://github.com/gafusion/gacode/commits/master/tglf, and the git commit ID is *5ab7221e*. The detailed settings of TGLF switches used in the predictive modelling for the JET D–T baseline (99 948) and hybrid (99 949) discharges are indicated by table 5. The TGLF switches not indicated in table 5 were set by the default values, which can be found in https://gafusion.github.io/doc/tglf/tglf_table.html.

Appendix C. QuaLiKiz settings

Table 6. QuaLiKiz switch setting used for the predictive simulation of JET D–T baseline and hybrid discharges in figure 6.

Switch	Definition	Setting in JINTRAC
qlk_rot_flag	2 is to impact of ExB shear stabilization only for $\rho > 0.5$	2
qlk_rhomax	QLK runs until the defined ρ and extrapolates as constant outside	0.85
qlk_rhomin	QLK runs from the defined ρ and linearly extrapolates to zero inside	0.03
qlk_usechieff	1 is to produce transport output as effective diffusion (0 = as diffusion and convection)	1
qlk_integration_routines	1 is to use cubature routines for integration routines	1
qlk_em_stab	1 is to use the ad-hoc model for EM stabilization effects	0

The QuaLiKiz version used in this paper is 2.8.2.

ORCID iDs

Hyun-Tae Kim https://orcid.org/0009-0008-2549-5624
Fulvio Auriemma https://orcid.org/0000-0002-1043-1563
Jorge Ferreira https://orcid.org/0000-0001-5015-7207
Stefano Gabriellini https://orcid.org/0000-0001-9488-5193
Aaron Ho https://orcid.org/0000-0001-5107-3531
Rita Lorenzini https://orcid.org/0000-0001-8353-4857
Michal Poradzinski https://orcid.org/0000-0002-1858-4046
Nan Shi https://orcid.org/0000-0001-7967-8778
Gary Staebler https://orcid.org/0000-0002-1944-1733
Žiga Štancar https://orcid.org/0000-0002-9608-280X
Gediminas Stankunas https://orcid.org/0000-0002-4996-4834
Vito Konrad Zotta https://orcid.org/0000-0002-3518-5178
Emily Belli https://orcid.org/0000-0001-7947-2841
Francis J Casson https://orcid.org/0000-0001-5371-5876
Jonathan Citrin https://orcid.org/0000-0001-8007-5501
Dirk van Eester https://orcid.org/0000-0002-4284-3992
Emil Fransson https://orcid.org/0000-0002-8747-3470
Daniel Gallart https://orcid.org/0000-0003-1663-3550
Jeronimo Garcia https://orcid.org/0000-0003-0900-5564
Luca Garzotti https://orcid.org/0000-0002-3796-9814
Joerg Hobirk https://orcid.org/0000-0001-6605-0068
Athina Kappatou https://orcid.org/0000-0003-3341-1909
Andrei Ludvig-Osipov https://orcid.org/0000-0002-7057-6414
Costanza Maggi https://orcid.org/0000-0001-7208-2613
Mikhail Maslov https://orcid.org/0000-0001-8392-4644
Massimo Nocente https://orcid.org/0000-0003-0170-5275
Par Strand https://orcid.org/0000-0002-8899-2598
Emmi Tholerus https://orcid.org/0000-0002-3262-1958

References

[1] Keilhacker M. *et al* 1999 *Nucl. Fusion* **39** 209
[2] Kim H.-T., Sips A.C.C., Challis C.D., Keeling D., King D., Joffrin E., Szepesi G., Buchanan J., Horton L.D. and Yuan X. 2020 *Nucl. Fusion* **60** 066003
[3] Horton L.D. *et al* 1999 *Nucl. Fusion* **39** 993
[4] Matthews G.F. 2011 *Phys. Scr.* **2011** 014001
[5] Beurskens M.N.A. *et al* 2013 *Plasma Phys. Control. Fusion* **55** 124043
[6] Kim H.-T., Romanelli M., Voitsekhovitch I., Koskela T., Conboy J., Giroud C., Maddison G. and Joffrin E. 2015 *Plasma Phys. Control. Fusion* **57** 065002
[7] Garzotti L. *et al* 2019 *Nucl. Fusion* **59** 076037
[8] Kim H.-T., Sips A.C.C., Romanelli M., Challis C.D., Rimini F., Garzotti L., Lerche E., Buchanan J., Yuan X. and Kaye S. 2018 *Nucl. Fusion* **58** 036020
[9] Challis C.D. 2022 Development of hybrid plasmas for D–T operation in JET *48th EPS Conf. on Plasma Physics in Geneva* ed European Physical Society
[10] Maggi C. *et al* 2023 Overview of T and D-T results in JET with ITER-like wall *Nucl. Fusion Special Issue: Overview and Summary Papers from the 29th Fusion Energy Conf. (London, UK, 16–21 October 2023)*
[11] Hawryluk R.J. 1981 An empirical approach to tokamak transport *Proc. Course Held in Varenna (Italy, 27 August–8 September 1979–1981)* pp 19–46
[12] PPPL TRANSP group TRANSP (available at: https://transp.pppl.gov/index.html)
[13] Romanelli M. *et al* 2014 *Plasma Fusion Res.* **9** 3403023
[14] Kalupin D. 2013 *Nucl. Fusion* **53** 123007
[15] Na Y.-S. *et al* 2019 *Nucl. Fusion* **59** 076026
[16] Mailloux J. 2022 *Nucl. Fusion* **62** 042026
[17] Garcia J. *et al* 2023 *Nucl. Fusion* **63** 112003
[18] Kim H.-T., Romanelli M., Yuan X., Kaye S., Sips A.C.C., Frassinetti L. and Buchanan J. 2017 *Nucl. Fusion* **57** 066032
[19] Garcia J., Challis C., Gallart D., Garzotti L., Görler T., King D. and Mantsinen M. 2017 *Plasma Phys. Control. Fusion* **59** 014023
[20] Garcia J. *et al* 2019 *Nucl. Fusion* **59** 086047

[21] Casson F.J. 2020 *Nucl. Fusion* **60** 066029
[22] Zotta V.K. *et al* 2022 *Nucl. Fusion* **62** 076024
[23] Goldston R.J., McCune D.C., Towner H.H., Davis S.L., Hawryluk R.J. and Schmidt G.L. 1981 *J. Comput. Phys.* **43** 61–78
[24] Pankin A., McCune D., Andre R., Bateman G. and Kritz A. 2004 *Comput. Phys. Commun.* **159** 157–84
[25] Štancar Ž. 2022 Interpretive modelling of fusion performance in JET DTE2 discharges with TRANSP *64th Annual Meeting of the APS Division of Plasma Physics* p O03.00012 (available at: https://meetings.aps.org/Meeting/DPP22/Session/PO03.12)
[26] Štancar Ž. 2023 Overview of interpretive modelling of fusion performance in JET DTE2 discharges with TRANSP *Nucl. Fusion* submitted
[27] Garzotti L. 2023 Development of high current baseline scenario for high deuterium-tritium fusion performance at JET *Nucl. Fusion* submitted
[28] Hobirk J. *et al* 2023 *Nucl. Fusion* **63** 112001
[29] Field A.R. *et al* 2021 *Plasma Phys. Control. Fusion* **63** 095013
[30] Garcia J. *et al* 2022 *Phys. Plasmas* **29** 032505
[31] Shimada M. *et al* 2007 *Nucl. Fusion* **47** S1
[32] Highcock E.G. 2010 *Phys. Rev. Lett.* **105** 215003
[33] Bourdelle C. 2018 *Nucl. Fusion* **58** 076028
[34] Tamor S. 1981 *J. Comput. Phys.* **40** 104
[35] Brambilla M. 1999 *Plasma Phys. Control. Fusion* **41** 1
[36] Hammett G.W. 1986 Fast ion studies of ion cyclotron heating in the PLT tokamak *PhD Thesis* Princeton University
[37] Kwon J.-M. 2007 Enhancement of NUBEAM for the simulation of fast ion and RF-wave interaction based on the quasi-linear theory *49th Annual Meeting of the Division of Plasma Physics* vol 52 (available at: https://meetings.aps.org/Meeting/DPP07/Event/71408)
[38] Kwon J.-M. 2006 Development of XGC-RF for global guiding-center particle simulation of minority ICRH heated plasmas in a general tokmak geometry *2006 48th Annual Meeting of the Division of Plasma Physics* (available at: https://meetings.aps.org/Meeting/DPP06/Event/53184)
[39] Eriksson L.-G., Hellsten T. and Willen U. 1993 *Nucl. Fusion* **33** 1037
[40] Challis C.D. Cordey J.G., Hamnén H., Stubberfield P.M., Christiansen J.P., Lazzaro E., Muir D.G., Stork D. and Thompson E. 1989 *Nucl. Fusion* **29** 563
[41] Gallart D. *et al* 2018 *Nucl. Fusion* **58** 106037
[42] Mantsinen M.J. *et al* 1999 *Plasma Phys. Control. Fusion* **41** 843
[43] Hirvijoki E. 2014 *Comput. Phys. Commun.* **185** 1310
[44] Asunta O.A., Govenius J., Budny R., Gorelenkova M., Tardini G., Kurki-Suonio T., Salmi A. and Sipilä S. 2015 *Comput. Phys. Commun.* **188** 33
[45] Van Eester D. and Lerche E.A. 2011 *Plasma Phys. Control. Fusion* **53** 092001
[46] Van Eester D. 2021 *J. Plasma Phys.* **87** 855870202
[47] Candy J., Sfiligoi I., Belli E., Hallatschek K., Holland C., Howard N. and D'Azevedo E. 2019 *Comput. Fluids* **188** 125
[48] Jenko F. 2000 *Phys. Plasmas* **7** 1904
[49] Weiland J., Jarmén A.B. and Nordman H. 1989 *Nucl. Fusion* **29** 1810
[50] Staebler G.M. 2007 *Phys. Plasmas* **14** 055909
[51] Staebler G.M. 2005 *Phys. Plasmas* **12** 102508
[52] Staebler G.M. 2021 *Nucl. Fusion* **61** 116007
[53] Bourdelle C. 2016 *Plasma Phys. Control. Fusion* **58** 014036
[54] Citrin J. *et al* 2017 *Plasma Phys. Control. Fusion* **59** 124005
[55] Connor J.W., Hastie R.J. and Taylor J.B. 1978 *Phys. Rev. Lett.* **40** 396
[56] Stephens C. 2021 Advances in quasilinear gyrokinetic modeling of turbulent transport *PhD Thesis* University of California Los Angeles
[57] Citrin J. *et al* 2022 *Nucl. Fusion* **62** 086025
[58] Waltz R.E., Casati A. and Staebler G.M. 2009 *Phys. Plasmas* **16** 072303
[59] Wang G. 2011 *Phys. Plasmas* **18** 082504
[60] Citrin J., Bourdelle C., Cottier P., Escande D.F., Gürcan Ö D., Hatch D.R., Hogeweij G.M.D., Jenko F. and Pueschel M.J. 2012 *Phys. Plasmas* **19** 062305
[61] Marin M. *et al* 2021 *Nucl. Fusion* **61** 036042
[62] Citrin J., Jenko F., Mantica P., Told D., Bourdelle C., Garcia J., Haverkort J.W., Hogeweij G.M.D., Johnson T. and Pueschel M.J. 2013 *Phys. Rev. Lett.* **111** 155001
[63] Mazzi S. 2022 *Nat. Phys.* **18** 776
[64] Garcia J. 2022 *Plasma Physcis Control. Fusion* **64** 104002
[65] Nabais F. 2010 *Nucl. Fusion* **50** 084021
[66] Kolesnichenko Y.I., Kim H.-T., Lutsenko V.V., Tykhyy A.V., White R.B. and Yakovenko Y.V. 2022 *J. Plasma Phys.* **88** 905880513
[67] Garcia J., Görler T. and Jenko F. 2018 *Phys. Plasmas* **25** 055902
[68] Auriemma F. 2023 TRANSP predictive modelling of DT JET baseline scenario *2023 EPS Conf. on Plasma Physics* (*Bordeaux, France*, *3–7 July 2023*)
[69] Zotta V.K. 2022 Predictive modelling of D-T fuel mix control with gas puff and pellets for JET 3.5 MA baseline scenario *48th EPS Conf. on Plasma Physics* (available at: http://ocs.ciemat.es/EPS2022PAP/pdf/P2a.115.pdf)